Land surface modeling over the Dry Chaco: The impact of model structures, and soil, vegetation and land cover parameters

Michiel Maertens[1], Gabriëlle J. M. De Lannoy[1], Sebastian Apers[1], Sujay V. Kumar[2], and Sarith P. P. Mahanama[2]

[1]KU Leuven, Department of Earth and Environmental Sciences, Belgium
[2]NASA Goddard Space Flight Center, Maryland, USA

Correspondence: Michiel Maertens (michiel.maertens@kuleuven.be)

Abstract. In this study, we tested the impact of a revised set of soil, vegetation and land cover parameters on the performance of three different state-of-the-art land surface models (LSMs) within the NASA Land Information System (LIS). The impact of this revision was tested over the South-American Dry Chaco, an ecoregion characterized by deforestation and forest degradation since the 1980s. Most large-scale LSMs may lack the ability to correctly represent the ongoing deforestation processes in this region, because most LSMs use climatological vegetation indices and static land cover information. The default LIS parameters were revised with (i) improved soil parameters, (ii) satellite-based interannually varying vegetation indices (Leaf Area Index and Green Vegetation Fraction) instead of climatological vegetation indices, and (iii) yearly land cover information instead of static land cover. A relative comparison in terms of water budget components and 'efficiency space' for various baseline and revised experiments showed that large regional and long-term differences in the simulated water budget partitioning relate to different LSM structures, whereas smaller local differences resulted from updated soil, vegetation and land cover parameters. Furthermore, the different LSM structures redistributed water differently in response to these parameter updates. A time series comparison of the simulations to independent satellite-based estimates of evapotranspiration and brightness temperature (Tb) showed that no LSM setup significantly outperformed another for the entire region, and that not all LSM simulations improved with updated parameter values. However, the revised soil parameters generally reduced the bias between simulated surface soil moisture and pixel-scale in situ observations, and the bias between simulated Tb and regional Soil Moisture Ocean Salinity (SMOS) observations. Our results suggest that the different hydrological response of various LSMs to vegetation changes may need further attention to gain benefits from vegetation data assimilation.

1 Introduction

Land surface models (LSMs) aim at providing a complete and self-consistent description of the temporal and spatial distribution of water and energy over land (Clark et al., 2015). The output from LSMs is used for many applications such as the monitoring of water resources, floods and droughts, and their impact on natural hazards, biomass production, ecology or soil salinity. In many cases, the LSM performance is improved by including remotely sensed observations through (i) the dynamic integration of observations into LSMs via data assimilation, (ii) the mapping of model input parameters to characterize the representation of land properties within the model (e.g., soil properties, land cover) and (iii) the validation and development of LSMs. In addition, contrasting model output with remote sensing is a powerful method to identify unmodelled processes in a LSM, such as irrigation (Kumar et al., 2015; Brocca et al., 2018), or groundwater withdrawal (Girotto et al., 2017). Furthermore, LSMs are an essential part of weather forecast systems and of climate models that simulate past, present and future climate (Pitman, 2003; Clark et al., 2015). They also offer ancillary information to decompose, inter- and extrapolate sparse ground measurements and remote sensing data. However, the degree to which LSMs can serve these various purposes depends on how well their given structure, forcing data and parameters can represent regional land surface processes (Wood et al., 2011; Clark et al., 2015). This study tests the impact of a revised set of soil, vegetation and land cover parameters on the performance of different LSMs.

Most LSMs use climatological or time-invariant parameters related to vegetation, land cover and soil properties and thereby assume stationary land processes, i.e. given similar meteorological input, the statistical distribution of the land surface variables would by design not change in time. These parameters can be properly calibrated for small-scale applications when suitable historical local data is available. However, for large-scale applications, it is common practice to provide the best possible, often satellite-based, large-scale input datasets to existing modeling systems (Jiang et al., 2010).

Satellite-based green vegetation fraction (GVF) and leaf area index (LAI) are example input datasets that directly or indirectly provide vegetation parameters (also referred to as vegetation indices) to represent the horizontal and vertical density of plant vegetation (Gutman and Ignatov, 1998), used for the calculation of transpiration, interception and radiative shading. Large-scale LSMs without dynamic vegetation modeling are strongly limited by the assumption that vegetation has a recurring annual cycle, i.e. using climatological LAI and GVF input. In reality, the vegetation's response to meteorological and climate conditions varies due to inter- and intra-annual weather and climate anomalies (Case et al., 2013).

The current abundance of satellite-based vegetation datasets allows to constrain LSMs and account for unmodeled processes in order to better understand the impact of vegetation changes on the water budget components. High-quality and long-term vegetation products from various remote sensing platforms (Tucker et al., 2005; Liang et al., 2013; Zhu et al., 2013) can provide temporally varying parametric input to LSMs (Boussetta et al., 2015). In addition, they can also be assimilated for state updating in LSMs with dynamic vegetation simulation (Sabater et al., 2008; Barbu et al., 2011, 2014; Albergel et al., 2017; Kumar et al., 2019). Earlier studies indicated that replacing climatological vegetation by interannually varying satellite-derived indices can improve modeled energy fluxes as well as surface temperature and moisture in both offline LSM simulations (Miller et al., 2006; Case et al., 2013; Yin et al., 2016) and atmosphere-coupled LSMs (Crawford et al., 2001; James et al., 2009; Boussetta et al., 2013; Ge et al., 2014; Kumar et al., 2014). The largest improvements are obtained during extreme meteorological anomalies (Case et al., 2013). In this study, it is expected that besides meteorological anomalies, also large-scale land cover conversions, such as deforestation, alter the vegetation strongly from its climatological representation. Therefore, it is tested if the use of satellite-derived vegetation indices in LSMs is also gainful in regions characterized by land cover changes.

Besides temporally varying vegetation indices, also a temporal varying description of land cover is required over regions with major land cover change. In LSMs, land cover is represented by the use of plant functional types (Kumar et al., 2006; Peters-Lidard et al., 2007). These are groups of plant species that share similar structural, phenological, and physiological traits (Bonan et al., 2002a). These features are integrated into several model-specific surface parameters for each land cover type, summarized in lookup tables (Dickinson, 1995). The sensitivity of LSMs to plant functional types or land cover related parameters has been illustrated in both offline (Chen et al., 2014) and atmosphere-coupled LSMs (Pitman et al., 2009; Grossman-Clarke et al., 2010; Cao et al., 2015; Ruiz-Vasquez et al., 2020). Most of these studies solely focused on changes in model-specific surface parameters without taking into account changes in LAI or GVF. In contrast, this study aims at implementing large-scale land cover changes in LSMs by feeding them with both temporally varying vegetation indices and land cover parameters.

Soil properties also form a suite of crucial input parameters in LSMs (Dai et al., 2019). Most LSMs derive soil hydraulic properties (SHPs) from lookup tables or pedotransfer functions, using soil texture information. Different LSMs have different soil parameterizations and use model-specific, often historically tuned, SHPs. Dai et al. (2019) stated that popular soil datasets currently used in LSMs are often outdated or have limited accuracy. Furthermore, the derivation of SHPs from soil texture is highly uncertain (Wösten et al., 2001). At the global scale, there are only a few generally accepted global soil maps, such as the Food and Agriculture Organization (FAO) Soil Map of the World (FAO, 1971), the Harmonized World Soil Database (HWSD) product (FAO and ISRIC, 2012) and SoilGrids (Hengl et al., 2017). As shown by De Lannoy et al. (2014), the implementation of more accurate soil texture and related SHPs, can lead to reduced bias and error-estimates of soil moisture when compared to in situ surface soil moisture and even impact simulated runoff and evaporation estimates. During the last decade, several operational institutes have improved their soil parameters to enhance global land surface simulations (Balsamo et al., 2009; De Lannoy et al., 2014; Chadburn et al., 2015).

In this study, soil, vegetation and land cover parameters are updated in three LSMs. The study domain is the South-American Dry Chaco. The region covers parts of Argentina, Bolivia, and Paraguay (Vallejos et al., 2015) and is characterized by deforestation since the 1980s, now being one of the largest deforestation hotspots in the world (Hansen et al., 2013). These large-scale land cover conversions impact the local hydrology of the region. In natural circumstances, deep percolation of water towards groundwater is low or even absent due to intensive evapotranspiration of the original dry forest vegetation (Giménez et al., 2016; Jobbágy et al., 2020). After deforestation, Giménez et al. (2016); Magliano et al. (2017); Marchesini et al. (2017) and Nosetto et al. (2012) all observed increases in soil moisture and deep drainage, resulting in a rise of the groundwater table. If this trend of a rising water table continues, this may result in salt accumulation close to the soil surface and eventually result in reduced plant growth and soil degradation (Giménez et al., 2016).

Given the Dry Chaco's recent and large-scale deforestation history, it is a unique area to test the impact of temporally evolving vegetation and land cover parameters. It is expected that by feeding LSMs with time-varying vegetation and land cover, together with an updated set of soil parameters, the most accurate spatial and temporal representation of the Chaco's water distribution could be obtained. Additionally, it is hypothesized that the use of similar soil, vegetation and land cover parameters in various LSMs, would result in similar accurate estimates of the long-term simulated water budgets. Lastly, it is hypothesized that soil and vegetation parameter updates would contribute differently towards the model performance improvement.

The general objectives of this study are: (i) to evaluate the simulated water budget components over the Dry Chaco using three different LSMs within the NASA Land Information System (LIS), (ii) to quantify how the simulated water budget components respond, when more accurate soil texture and related SHPs are implemented, or when the static climatological vegetation (LAI and GVF) indices and land cover map are replaced by interannually varying satellite-based indices and yearly updated land cover maps, and (iii) to identify the remaining deviations in the modeled hydrology compared to different satellite-based and in situ observations of water budget components. Besides these general objectives, the simulated water budget components are further framed within the hydrological context of the Dry Chaco, i.e. it is verified if the different LSMs simulate the increased deep percolation and higher soil moisture values after deforestation, similar to the field-based findings of Nosetto et al. (2012); Giménez et al. (2016); Magliano et al. (2017) and Marchesini et al. (2017).

The impact of the revised set of soil parameters and updated vegetation and land cover treatment is analyzed incrementally. In a first phase, models were run with their default model-specific soil parameters, climatological vegetation (LAI and GVF) and static land cover. Next, the models were supplied with more accurate soil texture and related SHPs and their impact on the simulated water budgets was quantified. In a third phase, the ongoing land cover changes were implemented using interannually varying satellite-based indices and yearly updated land cover maps and it was analyzed how the major land cover changes alter the hydrological balance. Lastly, the impact of the various model structures, soil texture and dynamic vegetation input was assessed using the concept of 'efficiency space' and the performance of each set of experiments was evaluated against independent satellite-based estimates of evapotranspiration, brightness temperature and in situ soil moisture.

2 Study area, models and datasets

2.1 Study area

The Dry Chaco is a relatively flat plain covering parts of northwestern Argentina, western Paraguay and southeastern Bolivia and has an area of approximately 787,000 km^2. The ecoregion has a semi-arid climate with a north-south gradient in the mean annual temperature (from 24°C to 19°C) and annual rainfall (from 898 mm/year to 712 mm/year) (Marchesini et al., 2020). Minetti et al. (1999) reports precipitation values up to 1000 mm/year in the eastern and western parts of the region and 400 mm/year in the central Dry Chaco. Soils in the Dry Chaco are the result of alternating aeolian and alluvial deposits whereby loess is prevailing. Field dunes and paleochannels with coarse sediments are common in the western Dry Chaco (Marchesini et al., 2017). The Dry Chaco hosts the largest dry forest in the world and historically, land use in the region was limited to extensive cattle ranching and semi-industrial or manual logging for timber and charcoal (Clark et al., 2010). Since the 1980s, the region is characterized by large-scale deforestation for soy-bean production and intensive cattle ranching (Vallejos et al., 2015). The region had the world's highest rate of subtropical forest loss between 2000 and 2012 and already 20% of the original dry forest in the region has been lost (Hansen et al., 2013; Vallejos et al., 2015), with a transformation of 158,000 km^2 between 1976 and 2012. Marchesini et al. (2017) mentioned agricultural and technological evolution together with growing international demand for grain as some of the causes of the agricultural expansion. In addition, gradual changes in forest structure, biomass and functioning are observed due to forest logging and forest grazing.

Figure 1 shows the location of the Dry Chaco, together with the spatial and temporal extent of land cover changes for the period 1992-2015 derived from the European Space Agency-Climate Change Initiative (ESA-CCI) land cover product upscaled to a 0.125° resolution (see section 2.3.3). The derived spatio-temporal pattern of deforestation agrees well with the 30 to 60 m resolution deforestation product of Vallejos et al. (2015) (not shown). The deforested area of the Dry Chaco in the overlapping period (1992-2013) of both products is 23% for the 0.125° ESA CCI data and only 15% for the finer-scaled dataset of Vallejos et al. (2015). The main reason for this discrepancy is the different spatial resolution of both products.

2.2 Models

Three LSMs within the NASA LIS (Kumar et al., 2008) were selected to simulate land surface states and fluxes over the Dry Chaco: the Community Land Model version 2 (CLM2.0) (Bonan et al., 2002b; Oleson et al., 2004), Catchment LSM-Fortuna 2.5 (CLSM-F2.5) (Koster et al., 2000) and Noah LSM version 3.6 (Ek et al., 2003), hereafter simply referred to as CLM, CLSM and NOAH, respectively. More recent versions of these models are available and might provide better simulations over the Dry Chaco, but are not yet implemented in LIS. This study relied on LIS to facilitate a consistent parameter revision across multiple LSMs and one of the main goals was to see the impact of various LSM structures, regardless of their version. To demonstrate the impact of the updated soil treatment and dynamically evolving vegetation and land cover, a baseline simulation for each LSM was conducted and followed by various revised experimental runs. For all simulations, the spatial resolution was 0.125° and the output was created daily (model integration timestep of 15 min). The LSMs were spun up for 10 years from 1 January 1982 through 31 December 1991 using the land cover of 1992. The subsequent simulations from 1 January 1992 through 31 December 2015 were used for further analysis. The meteorological forcing data (precipitation, temperature, specific humidity, radiation, wind and surface pressure) were extracted from the Modern-Era Retrospective analysis for Research and Applications (MERRA-2) product (Gelaro et al., 2017) including gauge-based precipitation corrections (Reichle et al., 2017).

By default, the LIS LSMs use climatological LAI data based on a 4-year average derived from the Moderate Resolution Imaging Spectroradiometer (MODIS) Collection 4 LAI product (Kaufmann et al., 2000), and climatological global GVF data (Gutman and Ignatov, 1998) derived from 5 years of normalized difference vegetation index (NDVI) data from the Advanced Very-High-Resolution Radiometer (AVHRR) (Miller et al., 2006). The default land cover map is the University of Maryland (UMD) global land cover product (Hansen et al., 2000) based on AVHRR data from 1 April 1992 through 31 March 1993. The default soil properties in LIS are derived from the FAO Soil Map of the World (FAO, 1971). In this study, vegetation, land cover and soil input data were revised using the Global Land Surface Satellite (GLASS) LAI (Liang et al., 2013; Xiao et al., 2016), the Global Inventory Modelling and Mapping Studies (GIMMS) NDVI (Tucker et al., 2005; Pinzon and Tucker, 2014), the ESA-CCI land cover product (Kirches et al., 2014; ESA, 2017) and soil properties derived from the HWSD v1.2 (FAO and ISRIC, 2012; De Lannoy et al., 2014).

2.3 Revised input data

2.3.1 GLASS LAI

The GLASS LAI product is a global spatio-temporally complete dataset, based on MODIS and AVHRR reflectance time series data (Liang et al., 2013). This product is available for the period 1981-2015, with a temporal resolution of eight days and a spatial resolution of 0.05° (Liang et al., 2013). Cloud-contaminated data are filled in using an optimum interpolation algorithm (Xiao et al., 2016). According to Liang et al. (2013) and Xiao et al. (2016), the GLASS LAI features more realistic and smoother seasonal variations than the MODIS LAI product (MOD15) (Knyazikhin et al., 1998) and the first version of the Geoland2 (GEOV1) LAI product (Baret et al., 2013). For the baseline simulations, a climatological LAI dataset was created using 24 years of GLASS data (1992-2015) to replace the default 4-year AVHRR climatology. This allowed to solely display the effect of interannual and short-term vegetation variations in the revised experiments with time-varying GLASS data and land cover changes. The LAI observations were upscaled to the 0.125° resolution by spatial averaging.

2.3.2 GIMMS NDVI

The GIMMS NDVI product was assembled from AVHRR NDVI data (Tucker et al., 2005). The GIMMS dataset covers the period 1982-2015 and has a 15-day temporal resolution. The spatial resolution is 0.0833°. The maps are 15-day maximum value composites and cloud-contaminated pixels are replaced by NDVI-values derived from either spline interpolation or average season profiles (Pinzon and Tucker, 2014). In this study, the GIMMS GVF was derived from its NDVI and used as input for the LSMs. According to Gutman and Ignatov (1998), the $GVF_{i,j}$ (-) is given by the following equation:

$$GVF_{i,j} = \frac{NDVI_{i,j} - NDVI_{min}}{NDVI_{max} - NDVI_{min}} \tag{1}$$

where $NDVI_{i,j}$ is the NDVI value observed at time i and pixel j and $NDVI_{min}$ and $NDVI_{max}$ are NDVI values over barren vegetation classes and fully covered vegetation classes, respectively. For simplicity, we chose to use the values proposed by Gutman and Ignatov (1998), i.e. 0.04 for $NDVI_{min}$ and 0.52 for $NDVI_{max}$, and the GVF is restricted to the 0-1 interval. Multiple other approaches exist to derive GVF from NDVI, each with their own advantages and limitations (Jiang et al., 2010). For the baseline simulations, a climatological GVF dataset was created using 24 years of GIMMS GVF data (1992-2015). For the revised experiments with inclusion of land cover changes, the time-varying GIMMS data were used. To match the model's 0.125° resolution, NDVI values were upscaled by spatial averaging.

2.3.3 ESA-CCI land cover

The ESA-CCI land cover product offers yearly varying information on 37 land cover classes from 1992 through 2015 at a spatial resolution of 300 m (Kirches et al., 2014; ESA, 2017). This long-term land cover time series was achieved by combining surface reflectance data of different observation systems (Medium Resolution Imaging Spectrometer (MERIS), AVHRR, , Satellite Pour l'Observation de la Terre (SPOT) Vegetation and PROBA-V)(Bontemps et al., 2012; Kirches et al., 2014). In this study, the ESA-CCI land cover maps were reclassified into 13 UMD classes (see Appendix 1) and upscaled to a 0.125° resolution assigning the most dominant land cover to each pixel. Figure 1 shows how deforestation in the Dry Chaco has progressed both in time and space, based on this ESA-CCI land cover information. A static water mask file was created based on pixels that were classified as water at least once during the period 1992-2015. For CLSM, the UMD land cover classes were further combined into model specific classes.

2.3.4 HWSD soil texture and SHPs

The global 1 km soil texture data were taken from the Soil and Terrain database for Latin America and the Caribbean as part of the HWSD v1.21 and were translated to 0.125° dominant soil texture. Similar as in De Lannoy et al. (2014), the soil texture and organic matter data was used to estimate SHPs using the pedotransfer functions of Wösten et al. (1999). The derived SHPs include the soil porosity, bulk density, Clapp-Hornberger parameter B, saturated hydraulic conductivity, saturated matric potential, soil wilting point and field capacity (see section 3.2.1). These HWSD-based soil parameters are also used in the operational Soil Moisture Active Passive (SMAP) Level 4 soil moisture product (Reichle et al., 2019).

2.4 Evaluation data

Precipitation input, and surface soil moisture and evapotranspiration output were evaluated against in situ measurements and satellite-based estimates. Furthermore, an integrated evaluation of surface soil moisture, surface temperature and LAI was performed through the comparison of diagnosed L-band brightness temperature (Tb) simulations against satellite-observed Tb obtained from Soil Moisture and Ocean Salinity (SMOS).

2.4.1 Precipitation

The quality of the MERRA-2 precipitation over the Argentinean Chaco was evaluated against in situ data obtained from the Instituto Nacional de Tecnología Agropecuaria (INTA, 2020). Two sets of daily precipitation data were downloaded: data from meteorological stations covering the period 1992-2015 (10 stations) and data covering the period 2010-2015 (8 stations). The exact location of these stations are shown in Figure 1. As this study mainly focused on long-term simulations, the precipitation evaluation was conducted using monthly-averaged data.

2.4.2 Monte Buey soil moisture

Pixel-scale in situ surface soil moisture was obtained from 17 nodes of the Monte Buey soil moisture network. The network is located in fields surrounding the town of Monte Buey, Cordoba, Argentina, just outside the Dry Chaco (Figure 1), and covers three 0.125° model pixels. At each node, the surface soil moisture is measured using a Hydra Probe II buried at a depth of 5 cm. The network adopts the highest quality standards (Thibeault et al., 2015) and serves as a calibration and validation site for various satellite missions, such as e.g. the SAtélite de Observación COn Microondas and SMAP. To allow for comparison with the daily modeled surface soil moisture, averaged over three 0.125° model pixels, the hourly in situ measurements were averaged to daily values across the 17 nodes. The period of validation was from 1 January 2013 through 31 December 2015.

2.4.3 Evapotranspiration

The modeled evapotranspiration components were evaluated against Global Land Evaporation Amsterdam Model (GLEAM) data. The GLEAM model consists of a set of algorithms that are driven by satellite-based observations and globally estimate all the daily evapotranspiration components at 0.25° spatial resolution (Miralles et al., 2011; Martens et al., 2017). Central in the GLEAM model is the use of the modified Priestley and Taylor (1972) equation. Daily LIS simulations of latent heat flux were upscaled to 0.25° to allow for comparison to GLEAM data for the entire simulation period, i.e. 1992-2015.

2.4.4 L-band microwave brightness temperature

The satellite-observed L-band Tb data was extracted from the SMOS SCLF1C product, version 620, projected onto the 36-km Equal-Area Scalable Earth Grid, version 2 (EASEv2), angular fitted and quality controlled as in De Lannoy et al. (2015), e.g. excluding areas close to open water, urban areas, with high radiofrequency interference, or with a poor angular fit. Both the horizontally (H) and vertically (V) polarized data at a 40° incidence angle were used for evaluation of the daily simulations (see section 3.5) from 1 January 2011 through 31 December 2015, using both ascending (6 am) and descending (6 pm) half-orbits.

3 Methodology

Table 1 summarizes the different experiments that were performed for each of the three selected LSMs. The experiments include a baseline (BL) simulation and two revised simulations, one with updated soil parameters (REV_S) and one with both updated soil, vegetation and land cover parameters (REV_{SV}), and two sensitivity simulations ($SENS_V$, $SENS_{LC}$), which are explained in section 3.2.3.

3.1 Baseline simulations

The set of baseline (BL in Table 1) simulations used the default FAO surface soil texture data and the related default model specific SHPs, assuming a vertically homogeneous soil profile for CLM and NOAH. By design, CLSM uses the 0-30 cm soil texture to compute parameters related to surface water transport, whereas the 0-100 cm soil texture is used for computation of all other parameters (Ducharne et al., 2000; De Lannoy et al., 2014). The vegetation input for the BL simulations consisted of monthly climatological vegetation datasets newly created based on GLASS LAI and GIMMS GVF, together with the ESA-CCI 1992 land cover map. This specific setup with climatological vegetation and static land cover does not account for major interannual changes in vegetation, such as e.g. due to deforestation. Note that CLM only requires LAI data, and GVF is not an input parameter.

3.2 Simulations with updated parameters

3.2.1 Revised soil parameters

In a first set of revised experiments, we replaced the model-specific SHPs (derived from FAO surface texture) for each LSM by the ‘topsoil’ SHPs associated with a vertically homogeneous 0-100 cm HWSD soil texture and organic matter similar as in De Lannoy et al. (2014). Corresponding to the default structure of CLSM, only the 0-30 cm HWSD soil texture is used to obtain model-specific parameters for the surface soil water transport. In these experiments, only the soil parameters were revised (REV_S in Table 1), whereas the climatological vegetation and land cover information was the same as in the BL

simulations. Our hypothesis was that by feeding the different LSMs with similar SHPs, differences between model output could be reduced.

It is important to note that the different LSMs do not use the same subsets of SHPs. By default, CLM uses pedotransfer functions (Cosby et al., 1984) to relate sand and clay fractions to SHPs. The used SHPs in CLM are the saturated conductivity (K_{sat}), porosity (θ_{sat}), the Clapp-Hornberger parameter B, and the saturated matric potential (ψ_{sat}) (Han et al., 2014). The soil profile is divided into 10 layers and K_{sat} decreases exponentially with depth throughout those layers.

CLSM's soil parameterization differs fundamentally from the other two LSMs. It uses several model parameters and moisture deficit model prognostic variables to dynamically partition the computational pixel into 3 distinctly different moisture regimes (saturated, transpiring and wilting regimes) to account for spatial variability of soil moisture within that pixel. CLSM's soil parameterization uses the spatial distribution of topographic indices and SHPs to derive model parameters (Ducharne et al., 2000). For baseflow generation only, CLSM assumes an exponential decay of K_{sat} with depth, with the decay factor ν=2.17 in the BL simulations and ν=1 in the REV_S simulations. Whereas for the vertical moisture transport, CLSM assumes K_{sat} to be vertically homogenous. Other important SHPs in CLSM are ψ_{sat}, the parameter B and soil wetness at wilting point θ_{wilt}.

The soil parameters in NOAH are discussed by Kishné et al. (2017) and the default SHPs are calculated from texture-based lookup tables (Cosby et al., 1984). The SHPs include the parameter B, θ_{sat}, ψ_{sat}, and K_{sat}. The soil profile is divided into 4 layers but with a constant K_{sat} value over depth (Ek et al., 2003). Other parameters include the soil water content threshold for ceasing evaporation from the top soil layer (DRYSMC), the saturated hydraulic diffusivity (SATDW), the soil water content at field capacity (REFSMC), soil wetness at wilting point θ_{wilt}, parameter for soil thermal diffusivity (F11) and quartz content (QTZ). Note that DRYSMC, SATDW, F11 and QTZ are not included in the SHPs of De Lannoy et al. (2014), and their values for the revised SHPs were derived from lookup tables based on the HWSD soil texture data.

The spatial boxplots in Figures 2a-c show three SHPs used in the BL simulations of each LSM and their updated values used for the REV_S and REV_{SV} simulations over the Dry Chaco. The mean values for the updated B parameter, θ_{sat} and ψ_{sat} are smaller than for BL, but have larger spatial variances. The slightly higher mean and standard deviation in the associated HWSD 0-100 cm sand fraction map (REV_S: 43±25%, Figure 2e), compared to that of the FAO surface sand fraction map (BL: 41±15%, Figure 2d), explain the change of these updated parameter values.

3.2.2 Revised vegetation and land cover parameters

To analyze the response of the Chaco's hydrology to deforestation or vegetation changes in general, time-varying vegetation observations from GLASS and GIMMS were incorporated into the LSMs together with yearly updated ESA-CCI land cover maps in a second set of revised experiments (REV_{SV} in Table 1). This specific setup includes the effect of vegetation changes (such as deforestation) compared to the use of climatological vegetation parameters and static land cover in the BL simulations. As described in sections 2.3.1 and 2.3.2, the GLASS LAI and GIMMS NDVI were available every 8 and 15 days, respectively. However, the data were linearly interpolated to obtain daily parameter updates in LIS. The ESA-CCI land cover maps were updated each year on 1 January. LSMs only use land cover information to define model-specific parameters associated to each land cover type, i.e. ESA-CCI land cover is used as predictor of parameters such as rooting depth, stomatal conductance and surface roughness. The exact values and implementation of each parameter is model-dependent.

Note that albedo calculations in each model were kept unchanged, as the focus of this study is primarily on the water balance. In CLM, the albedo for vegetated areas is calculated based on soil properties, LAI and plant functional types (Oleson et al., 2003). CLSM uses a surface albedo parameterization scheme (based on the Simple Biosphere Model, (Sellers et al., 1986)) that incorporates LAI, GVF and sun incidence angle to calculate the albedo and is rescaled to fit the annual cycle of MODIS-observed albedo. NOAH uses an albedo climatology based on 5 years (1985-1989) of visible and near-infrared radiation from AVHRR (Csiszar and Gutman, 1999). To see how deforestation influences the water budget component, the water budget analysis of the REV_{SV} output mainly focused on the subset of 197 pixels that were deforested between 2002 and 2006 (based on the ESA-CCI land cover).

3.2.3 Sensitivity experiments

Our results will indicate (see section 4.1.3) that the various LSMs react differently to the simultaneously updated interannually varying vegetation and land cover parameters. To disentangle the impact of vegetation and land cover parameters separately for each LSM, two sets of synthetic sensitivity experiments were conducted. A first set of sensitivity experiments ($SENS_V$ in Table 1) included 5 experiments (‘exp1’ through ‘exp5’) in which monthly spatially distributed climatological GLASS LAI values of the BL simulations were systematically increased by one and GVF values were raised proportionately. To estimate the corresponding GVF values, an empirical exponential relationship between LAI and GVF ($GVF = a + (b * exp(c * LAI))$) was derived for each individual pixel based on daily LAI and GVF values from 1992 to 2000. LAI values much larger than about six do not occur in reality, nevertheless they are kept in this sensitivity analysis to understand the LSM response in a synthetic setting. In CLM only the LAI was altered because CLM does not use GVF as an input, whereas both LAI and GVF were altered in CLSM and NOAH. Each experiment was run for the years 1992-2015 with a fixed ESA-CCI land cover map of 1992.

To test the sensitivity to land cover ($SENS_{LC}$ in Table 1), two simulations were conducted per LSM. In a first simulation, the entire Dry Chaco was assumed to be covered by deciduous broadleaf forest, whereas in the second scenario cropland was assumed. These vegetation classes are associated with the major land cover conversion in the Dry Chaco. The climatological GLASS LAI and GIMMS GVF datasets were used in $SENS_{LC}$ simulations.

3.3 Model evaluation in terms of water budget components

To assess the relative impact of different LSM structures, vegetation and land cover parameters, various water budget components were compared in each simulation:

$$P = ET + Q + \Delta S \tag{2}$$

where P is the precipitation [mm], ET is the total evapotranspiration [mm], Q is the total runoff [mm], and ΔS is the change in soil water storage [mm] for a given time period. The total ET and Q in the water budget equation (2) can be written as the sum of their different components:

$$ET = E_V + E_B + E_I \quad (3)$$

$$Q = Q_S + Q_{SB} \quad (4)$$

where E_V is the vegetation transpiration [mm], E_B is the bare soil evaporation [mm], E_I is the evaporation from canopy interception [mm], Q_S is the surface runoff [mm], and Q_{SB} is the subsurface runoff [mm].

3.4 Model evaluation with efficiency curves

The relative differences in the various LSM behaviors were further analyzed using efficiency curves, without associating any performance assessment. Q and ET are strongly regulated by soil moisture. However, soil moisture is also a highly model-dependent quantity (Koster et al., 2009), complicating the evaluation of the modeled Q and ET. To avoid this issue, Koster et al. (2012) and Koster (2015) proposed to evaluate hydrological behavior in terms of 'efficiency space'. The main reasoning behind this approach is that higher soil moisture content generally leads to both increased ET for a given amount of net incoming radiation (ET efficiency) and increased Q for a given amount of P (Q efficiency). The ET efficiency [-] is the ratio of the latent heat flux to the net radiation:

$$\lambda ET / R_{net} = \beta(mc_{1m}) \quad (5)$$

where λ [J kg^{-1}] is the latent heat of vaporization, λET [J m^{-2}] is the latent heat flux, R_{net} [J m^{-2}] is net incoming radiation and $\beta(.)$ [-] is a function of moisture content, here assumed the 1 m soil moisture content mc_{1m}. The Q efficiency [-] is the ratio of the total Q production to the total P:

$$Q/P = F(mc_{1m}) \quad (6)$$

where Q is total runoff, P is the precipitation and $F(.)$ [-] again is a function of mc_{1m}. By plotting the Q efficiency against ET efficiency, and identifying their relationship, a unique signature of the hydrological behavior (without model-dependent soil moisture) of a LSM can be obtained. Ideally, this would allow to shift a LSM signature towards an in situ observed land surface signature. Due to lack of suitable and publicly available Q measurements for the Dry Chaco, this study uses the efficiency space to relatively compare the hydrological behavior of different LSMs with various parameter settings (BL, REV_S, REV_{SV}).

For each pixel, water budget components (λET, R_{net}, Q, mc_{1m} and P) were averaged over each month for the period 1992-2015. Different locations had different minimum mc_{1m} values, induced by differences in soil texture. Prior to plotting, the mc_{1m} values for each pixel were normalized to reduce spatial differences in mc_{1m} and to dominantly focus on the temporal LSM signature. Both the Q and ET efficiency were plotted in function of the normalized mc_{1m} for each LSM to visualize the model-specific soil moisture dependencies. For each pixel, a curve drawn through the points was constructed by computing the median of the ET and Q efficiency over narrow bins of normalized mc_{1m}. The combination of all fitted curves for all pixels was visualized using a scatter density cloud. The resulting 'efficiency space' plots (showing the obtained ET efficiency in function of Q efficiency) show how evaporation and runoff efficiencies vary with each other, as the soil gets drier or wetter. The efficiency plots are used to see if the three LSMs provide a consensus on the simulated hydrological behavior and on the impact of the updated soil, vegetation and land cover treatment.

3.5 Model evaluation with independent data

For each experiment, the quality of model input P, and the model performance in terms of output surface soil moisture content (sfmc) and ET were evaluated against independent data (section 2.4), for simplicity referred to as 'observations', using four skill metrics:

- Bias: long-term mean difference between simulations and observations (i.e., model minus observation),
- ubRMSD: unbiased root-mean-square difference, calculated by first removing the bias from both the simulated and observed time series (Entekhabi et al., 2010),
- R: temporal Pearson correlation coefficient between simulations and observations,
- aR: temporal anomaly Pearson correlation coefficient between simulations and observations, calculated after removing the mean climatology from each time series. The climatology is computed as the multi-year average of 30-day smoothed time series of daily values. This removed the trivial agreement in seasonality and allowed to the focus on interannual and short-term dynamics.

For an integrated evaluation of the model sfmc, surface temperature and LAI of the various experiments, a zero-order tau-omega microwave Radiative Transfer Model (RTM) was used to convert these modeled variables into L-band Tb [K] estimates. The modelled Tb were compared to SMOS Tb observations, similar to the approach presented by Albergel et al. (2012). For a detailed description of the tau-omega RTM we refer to De Lannoy et al. (2013). Feldman et al. (2018) showed that a zero-order tau-omega model would suffice for the dry forests of the Dry Chaco. Instantaneous sfmc, surface temperature and LAI at 6 am and 6 pm were used as input in the RTM and simulated Tb were evaluated against 6 am and 6 pm SMOS-observed Tb (both at the top of vegetation). The Tb simulations were computed at the 0.125° model resolution and then spatially averaged to the 36-km EASEv2-grid for comparison to SMOS-observed Tb for the period 2011-2015. Short-term variability in both simulations and observations was reduced using a 1-month averaging window. This allowed to focus on the effect of the implemented vegetation changes, which occur on a longer seasonal timescale.

The RTM required specific input parameters related to soil properties (Wang and Schmugge, 1980) and vegetation classes. The related soil parameters differ thus for the BL and REV_S simulations, and the parameters related to land cover class also vary in time for the REV_{SV} simulations due to yearly updated land cover. The literature offers various lookup tables to estimate the RTM parameters related to vegetation classes (soil roughness, scattering albedo, vegetation structure parameters). Here, we used the lookup tables of the SMAP soil moisture retrieval (O'Neill et al., 2015; Quets et al., 2019). Another choice would affect the overall Tb bias for all experiments, but would minimally affect the relative comparison of the various experiments with revised soil and vegetation parameters.

4 Results

4.1 Model evaluation in terms of water budget components

4.1.1 Baseline simulations

The annual and seasonal distribution of the different water budget components for each BL model simulation is summarized in Table 2. The values are calculated for a 24-year period (1992-2015) and averaged over all pixels within the Dry Chaco, excluding open water pixels. The Dry Chaco receives an average yearly P of 809 mm with most P (643 mm) during the wet season (October-March), in line with the findings of Marchesini et al. (2020) and Minetti et al. (1999). All LSMs confirm a water storage (ΔS) deficit for the dry season (April-September), which is compensated during the wetter months with a water surplus. Figure 3a shows the corresponding yearly averaged water budget components relative to the total P whereby the total ET is subdivided in its three components (see section 3.3). The variation in the total amount of ET and its components shows that there is large variability between the models, even though all of them use the same forcing data, land cover, vegetation, soil texture (not SHP) and topography input. In addition, there are significant disagreements in the ET partitioning. The largest ET component is different in each LSM, i.e. E_I is largest for CLM, E_B for CLSM and E_V for NOAH. The high fraction of E_I for CLM is physically unrealistic (see section 5). CLM and NOAH both have a Q_{SB} component, whereas CLSM does not. The latter has a very large fraction of Q_S.

4.1.2 Revised soil parameters

The impact of the revised soil parameters (REV_S) on the yearly mean relative water budget components is shown in Figure 3b, again for the period 1992-2015. Most striking is that, despite the similarity in SHPs, the various models still produce a very different partitioning of the water budget components. For CLM, the revised SHPs cause a yearly reduction in Q_S by 4% which is compensated by an increase in E_V and Q_{SB}. For CLSM, the mean water budget components hardly changes. For NOAH, there is a small increase in Q_{SB} and decrease in ET, mainly due to a large decrease in E_B (-9%) of which 6% is compensated by extra E_V. For each model, the differences in the water budget components between the BL and REV_S simulations, averaged over the entire Dry Chaco, are relatively small. However, within the study domain, there is a large local spatial variability in the changes of the various water budget components (not shown).

Figure 4 summarizes the impact of the updated SHPs on the soil moisture content in the first meter of the soil (mc_{1m}). The boxplots of time-averaged (1992-2015) mc_{1m} over the Dry Chaco (Figure 4a) show that the REV_S simulations are drier than for BL: the mc_{1m} decreases from 0.16 to 0.11 m^3/m^3 for CLM, from 0.22 to 0.13 m^3/m^3 for CLSM and from 0.19 to 0.17 m^3/m^3 for NOAH. These lower mean soil moisture values can be related to the larger fraction of sandy soils (Figures 2d and e) and the associated reduced water retention (SHPs) in the REV_S simulations. However, again, at the local scale, some areas become wetter and others drier. Despite the relatively large difference in long-term mean soil moisture between BL and REV_S, the differences in ET and Q_S fluxes are small: the meteorological forcings are the primary drivers of these fluxes, whereas the SHPs only have a secondary impact. Figures 4c and 4d show how the texture pattern dominates the long-term averaged mc_{1m} for the period 1992-2015 for the NOAH BL and REV_S simulations (similar for CLM and CLSM). Figure 4b illustrates that the updated SHPs change the temporal standard deviation of mc_{1m}, which significantly decreased for NOAH.

4.1.3 Revised vegetation and land cover parameters

The impact of deforestation over the Dry Chaco was assessed via a relative comparison of the water budget components of the REV_S and REV_{SV} simulations for each LSM, using a subset of 197 pixels that were deforested between 2002 and 2006. Keep in mind that the REV_S uses climatological vegetation indices and a static land cover map, which do not account for interannual vegetation changes. The REV_{SV} simulations include the effects of vegetation changes by the implementation of satellite derived dynamic vegetation indices as well as yearly updated land cover parameters. The differences between the REV_S and REV_{SV} simulations thus solely stem from interannual vegetation variations and land cover changes. By design, the former would only introduce minimal long-term differences over the entire simulation period. Therefore, the output differences were only analyzed after deforestation, i.e. for the period 2007-2015. Figure 5 compares the water budget components for the REV_S and REV_{SV} simulations after deforestation, i.e. for the period 2007-2015. For CLM, we observed a relative decrease in E_V (-6%), that is compensated by an increase in E_B and E_I maintaining a constant amount of ET. For CLSM, there is a 5% decrease in total ET (with a similar relative distribution of the ET components), which is compensated by a Q_S increase of 5%. For NOAH, deforestation also resulted in smaller ET (-3%), which is compensated by an increase in Q_{SB}. Regarding the relative ET distribution of NOAH, there is an increase in E_B of 4% and a decrease in the E_V with 6%.

The impact of vegetation changes on the temporal evolution of LAI and moisture content in the first two meters of the soil (mc_{2m}) is illustrated in Figure 6 for a representative pixel (28.0625° S, 63.6875° W). Figure 6a shows the climatological REV_S LAI and the interannually varying REV_{SV} LAI, together with P for a pixel that was deforested in 2004 (based on ESA-CCI land cover). The LAI values are generally low both before and after deforestation. Years where the REV_{SV} LAI is larger than its climatology, mainly correspond to wetter years. Deforestation does not cause a sudden drop in LAI, probably because the LAI for fully developed crops is not very different from that of dry forests, or the smaller-scale deforestation signal may be suppressed in the upscaled 0.125° LAI values. However, the REV_{SV} LAI is significantly smaller than its climatology in drier years after 2004, which may be indicative of less crop cover and earlier deforestation. In short, the coarse resolution LAI does not necessarily reflect land cover changes and is strongly influenced by P.

The combined impact of time-varying LAI and land cover on mc_{2m} is shown in Figures 6b-d for the REV_S and REV_{SV} simulations of each LSM. From the deforestation in 2004 onwards, the mc_{2m} of the REV_{SV} simulations increases for each model, but at a different rate. The main driver for the increase in mc_{2m} is the change in land cover. The updated parameters related to a land cover change push the model out of its equilibrium and water is gradually redistributed to achieve a new balance with a higher soil moisture content. Considering all pixels deforested between 2002-2006, mc_{2m} increases on average by 0.0035 m^3/m^3 (maximum change of 0.016 m^3/m^3) for CLM, by 0.03 m^3/m^3 (maximum change of 0.08 m^3/m^3) for CLSM and by 0.07 m^3/m^3 (maximum change of 0.1 m^3/m^3) for NOAH. The reason for the different behavior of each LSM will be explained in the following paragraph.

4.1.4 Sensitivity experiments

Sensitivity experiments with synthetic vegetation and land cover parameter were conducted to get more insight into the distinct behavior of soil moisture for the different LSMs in response to dynamic vegetation and land cover input. Figures 7a-c illustrate how domain-averaged water budget components change when the LAI is systematically increased by 1 to 5 units ('exp1' through 'exp5') as explained in section 3.2.3. To mimic the effect of deforestation, assumed to result in smaller LAI values, one should read the figure from exp5 (high LAI) to exp1 (low LAI). For CLM, a reduction in LAI introduces a reduction in E_I, an increase in E_B and a slight decrease in E_V. For CLSM, a reduction in LAI and GVF yields a strong decrease in E_I, fully compensated by an increase in E_B whereas E_V is barely affected. Concerning NOAH, smaller LAI and GVF values result in a significant decrease in E_V. When the LAI and/or GVF are reduced, the Q_{SB} increases in both CLM and NOAH.

Figures 7d-f illustrate how the various LSM soil moisture profiles respond to changing LAI (and corresponding GVF for CLSM and NOAH). A decrease in LAI barely affects soil moisture in CLSM, whereas it increases soil moisture for CLM (moderately) and NOAH (strongly), in line with the respective LSM's degree of decrease in E_V (water extraction from the soil). The increase in soil moisture climatology for an imposed decrease in LAI (while assuming a persistent vegetation type) is partly an artifact resulting from a one-way dependency of soil moisture to vegetation in the absence of a dynamic vegetation growth module. In nature, LAI and soil moisture evolve together.

Figures 7g-i show soil moisture profiles for the sensitivity experiment in which the land cover was either uniformly cropland or forest. For CLM, there is almost no difference in soil moisture between both. CLSM has a slightly wetter soil moisture profile for cropland than for forest. For NOAH, the soil moisture content is higher under cropland than forest in the deeper layers. The distinct model response to land cover changes is related to the fact that each model uses a model-specific set of land cover parameters, each with different values and behavior. These parameters impact the total E_V (not shown) and the related water extraction from the soil. For example, the rooting depth (the depth to which roots of plants can extract water from the soil profile) is defined differently in each LSM. In NOAH, the forest land cover class has a rooting depth of 2 m, i.e. roots take up water over the whole profile. Roots of crop are parameterized to 1 m and are not able to extract water from the deepest soil layers, resulting in wetter soils at the bottom of the soil profile (Figure 7i). CLM makes use of a root fraction distribution whereby root fraction is a function of depth and land cover type as described in Zeng (2001). CLSM uses a rooting depth of 1 m, regardless of the land cover.

The sensitivity experiments were designed to explain the distinct behavior of soil moisture in response to changing land cover or vegetation parameters separately, and do not provide insights in possible interactions between both. The relative change in the water budget components of REV_{SV} against REV_S, as shown in Figure 5, originate from changes in LAI and GVF, land cover, and their interactions. This explains, for example, the increase in model Q_S and decrease in total ET after deforestation for CLSM. This cannot be explained by the CLSM results of the $SENS_V$ (Figure 7b) or $SENS_{LC}$ experiments alone.

4.2 Model evaluation with efficiency curves

4.2.1 Baseline simulations

To compare the BL hydrological behavior of the three different LSMs, Figure 8 presents the Q and ET efficiency in function of mc_{1m} along with the 'efficiency space'. For each pixel within the Dry Chaco, these quantities are computed for each month across the 24-year time period, and a curve is fitted using a simple binning procedure. Figure 8 summarizes the hydrological signature of the Chaco by showing the density scatter cloud of all fitted curves.

Figures 8a, d and g show a very different Q efficiency in function of mc_{1m} for the three LSMs. For CLSM, a majority of the curves reaches Q efficiencies values up to 0.4, whereas the median values are around 0.2 for CLM and even below 0.1 for NOAH. This different behavior was also observed in the annual water budget analysis (see Table 2). Note that for CLM and NOAH, some high Q efficiencies are found at relatively low mc_{1m} values (black circle). This is caused by high Q_{SB} rates, which allow precipitation from the wet season to run off during the dry season months even if P in the latter period is small.

For all LSMs, the ET efficiency (Figures 8b, e, h) is larger than the Q efficiency and the relationship of the ET efficiency with mc_{1m} is more similar across the three LSMs than that of the Q efficiency. The distinct BL signature of the three LSMs in efficiency space is summarized in Figures 8c, f, i and mainly explained by differences in Q.

4.2.2 Revised simulations

Figure 9 shows the impact of the REV_S and REV_{SV} experiments in efficiency space. The impact of the updated SHPs is summarized by a small shift between the mean values of the BL and REV_S in efficiency space, with a decrease in Q efficiency for CLM, and increase for CLSM and NOAH.

Figure 9 also shows the REV_S and REV_{SV} scatter density clouds (and mean value) in efficiency space for the 197 pixels deforested between 2002 and 2006 for the period 2007-2015. The inclusion of vegetation changes (REV_{SV}) causes a shift towards larger Q efficiencies for CLSM (increased Q_S) and NOAH (increased Q_{SB}). The opposite is found for CLM. When analyzing the effect of deforestation on ET efficiency, it is important to keep in mind that these efficiencies are calculated as the ratio of the latent heat flux to the net incoming radiation (available energy). By definition, the net radiation is also impacted by vegetation changes. Therefore, one cannot directly relate changes in ET efficiency to changes in total ET. For CLM, the REV_{SV} density cloud tends to larger ET efficiencies, indicating that croplands need less energy than forests for the same amount of ET. For CLSM and NOAH, the scatter cloud shows a slight shift to the right: croplands use a slightly larger portion of the available energy than forest for ET.

4.3 Model evaluation with independent data

4.3.1 Precipitation

Because the quality of input P will greatly influence the quality of ET, sfmc and Tb simulations, independent of the used LSM, the quality of the MERRA-2 P product was first evaluated against in situ P data. Table 3 summarizes how well the monthly averaged MERRA-2 P corresponds with in situ observations for two types of stations. For the 10 stations that cover the 1992-2015 period, the mean correlation coefficient is 0.83 ($\pm$ 0.07), the mean monthly bias is 5 ($\pm$ 11) mm/month and the mean ubRMSD equals 38 ($\pm$ 17) mm/month. For the 2010-2015 stations (n=8), the overall skill metrics are lower: a mean correlation of 0.74 ($\pm$ 0.11) a mean bias of 18 ($\pm$ 13) mm/month and a mean ubRMSD of 42 ($\pm$ 14) mm/month, respectively. The positive bias indicates that MERRA-2 P is overestimated.

4.3.2 Monte Buey soil moisture

Figure 10 shows daily modeled sfmc time series for CLM, CLSM and NOAH, together with in situ Monte Buey sfmc (5 cm) observations (both averaged over the three pixels) for the period 2013-2015. For CLSM and NOAH, the sfmc depth is 2 and 10 cm, respectively. For CLM, the soil moisture content in the 4 upper soil layers was averaged to obtain a 5-cm sfmc value.

The largest R and aR values between observed and modeled sfmc are obtained with CLM and NOAH (R and aR values between 0.72 and 0.81 for BL). By updating the soil parameters (REV_S), some R and aR values increase, but other decrease. However, the bias is decreased for all models. For NOAH, the updated soil parameters result in substantially wetter sfmc during the dry season. Note that these results are only valid for the three model pixels covering the Monte Buey site, and cannot be extended to the entire Dry Chaco.

4.3.3 Evapotranspiration

The skill of daily simulated total ET relative to that of GLEAM-based ET estimates is shown in Figures 11a-d for the period 1992-2015 over the entire Dry Chaco. In general, NOAH has the largest R and aR, and the smallest ubRMSD. When averaged across the entire region and time period, the impact of the updated soil, vegetation and land cover parameters on the total ET is negligible and even deteriorates the overall CLSM performance relative to GLEAM.

The relative distribution of the different ET components is very different for GLEAM than for the selected LSMs. Figure 11e shows that all models (REV_S) are possibly underestimating the E_V. For GLEAM, 89% of the total ET is E_V, whereas this is only 47% for NOAH, 31% for CLSM and 18% for CLM. E_I is the second largest component in GLEAM (7%). CLM (48%) and NOAH (27%) are likely overestimating the E_I, whereas CLSM overestimates the E_B.

4.3.4 L-band microwave brightness temperature

Time series of the simulated 40° Tb at horizontal polarization (Tb$_H$) with NOAH BL, REV_S and REV_{SV} input, and SMOS Tb$_H$ are shown in Figure 12a. The inputs used in the RTM for the simulated Tb include simulated surface soil moisture (using FAO texture and related SHPs in the BL simulations, HWSD based texture and SHPs in the REV_S and REV_{SV} simulations), temperature, LAI (climatological in BL and REV_S, interannually varying in REV_{SV}), land cover (static in BL and REV_S , yearly updated in REV_{SV}) and the associated literature-based look-up RTM parameters. These time series are for the 36-km EASEv2 pixel that includes the deforested 0.125° pixel shown in Figure 6. The corresponding sfmc and LAI are shown in Figures 12b and 12c. Time series of NOAH Tb at vertical polarization (Tb$_V$) and the simulations for CLM and CLSM showed similar behavior and are not shown. Figure 12 highlights how the REV_{SV} LAI deviates from the long-term climatology (REV_S) during the SMOS observation period. Not shown here is that the LAI also deviates from the climatology earlier in time, i.e. on average the interannual variations cancel each other out by design, as in Figure 6.

The updated soil parameters (REV_S) affect the sfmc and RTM parameters, causing a different behavior in simulated Tb_H. The reduced LAI and changes in land cover (REV_{SV}) result in wetter sfmc but the sfmc increase is not as pronounced as for the mc_{2m} in Figure 6d. This wetter sfmc and reduced LAI propagate through the RTM and result in colder simulated Tb_H.

Figures 13a-d summarize the Tb skill metrics for the different experiments, only for the subset of pixels that were deforested between 2002 and 2006. The metrics for both polarizations (Tb_H and Tb_V) were averaged before creating the spatial boxplots. In general, the Tb bias for each model is negative, indicating that the simulated Tb is colder than the SMOS Tb. NOAH has the largest absolute bias and the updated soil treatment reduces the Tb bias of each model. CLSM has the best R and aR values, but the updated soil parameters reduce its performance in terms of R, aR and ubRMSD values. This is in line with the reduced performance of CLSM relative to the GLEAM ET. For NOAH, the updated soil treatment increases the R and aR values, and reduces the ubRMSD. The additional impact of the updated vegetation and land cover treatment is small.

To visualize the local effects of the vegetation changes, spatial maps of the differences in temporal R values (ΔR) between the REV_{SV} and REV_S, are shown for each model in Figures 13e-g. The modeled Tb, and the spatial pattern of ΔR, over the Dry Chaco are mainly driven by changes in sfmc, and these are driven by vegetation and land cover changes. The ΔR values are relatively small for CLM because the model sfmc is only slightly sensitive to changes in vegetation and land cover parameters. For CLSM, the REV_{SV} simulations yield larger R values over certain areas compared to the REV_S simulations because temporal changes in modeled sfmc mainly result from changes in land cover parameters. Consequently, the ΔR pattern is similar to the deforestation pattern (see Figure 1). In NOAH, the sfmc is sensitive to land cover and LAI changes, and therefore, the ΔR pattern depends on both land cover and LAI changes. For NOAH, the ΔR values do not increase everywhere. At some pixels with reduced REV_{SV} performance, we noticed unexpected trends in the LAI time series (not shown), i.e. LAI would not show the expected decrease during the dry season. This possibly deteriorated the Tb simulations. In short, the extent of the simulated Tb response to vegetation and land cover changes is model specific and is mainly driven by the sensitivity of the model's sfmc to vegetation and land cover parameters.

5 Discussion

5.1 LSM comparison

The relative evaluation of LIS CLM, CLSM and NOAH in terms of their water budget components (Table 2 and Figure 3) and efficiency space (Figure 8) highlights that each LSM has a distinct hydrological signature. CLSM has more Q_S than NOAH and CLM, but CLSM has no Q_{SB} component, unlike NOAH and CLM. It is striking how the various LSMs partition the total ET very differently into its three components, as was reported before by Wang and Dickinson (2012); Kumar et al. (2018); Rigden et al. (2018); Zhang et al. (2020). For example, we found that CLM strongly overestimates the E_I and E_B compared to GLEAM over the Dry Chaco (Figure 11e). Lawrence et al. (2007) came to similar findings and indicated that by reducing the tuning parameter α_l from 1 to 0.25 in the canopy interception equation, the amount of E_I could be reduced to more realistic values at the global scale. They also indicated that the relative contribution of E_V and E_B in vegetated regions could be improved by altering two parameters ($C_{s,dense}$ and α) in the equation to calculate the turbulent transfer coefficient between the soil and canopy air. For CLSM, the portion of E_I over the Dry Chaco is similar to that of the GLEAM product. Reichle et al. (2011) described how the amount of interception evaporation is influenced by the rainfall interception parameters FWETL and FWETC, and that realistic interception rates are found when both parameters equal 0.02 (applied in our simulations). These parameters describe the fractional areas of canopy leaves (interception reservoir) on which large-scale and convective rainfall are applied. The bias between modeled ET and GLEAM is high for NOAH, indicating an overestimation of the total ET. Wei et al. (2013) observed that NOAH yields substantial biases in latent heat flux, total Q and land surface skin temperature when compared to independent data over the United States. They showed that adapting model parameterizations, such as including a seasonal factor for the root distribution and selecting optimal model parameters related to the canopy resistance calculations (an important factor for E_V simulation), could reduce these biases.

Our results show that constraining the LSMs with the same, optimal soil, vegetation and land cover parameter input (REV_S and REV_{SV}) does not result in more similar water budget partitioning, because the results are dominated by internal model-specific equations and parameters. The latter have historically been tuned globally with particular input datasets and may compensate for errors in those datasets, so that 'better' input does not necessarily lead to 'better' output. In addition, some LSMs are inherently more or less sensitive to time-varying parameters and therefore climatological vegetation input may suffice if the LSM is simply not very sensitive to vegetation changes (Jarlan et al., 2008), or if the vegetation changes are not extensive. LSMs could benefit from further development to obtain a more realistic hydrologic response to vegetation changes and to better include dynamic vegetation phenology. This should lead to more realistic simulations of the interaction between the carbon and water cycles.

Lack of sufficient in situ Q and ET measurements over the Dry Chaco, prevents to identify which LSM setup best approaches the long-term observed water budget and its components. However, our study highlights the large estimation uncertainty due to model structures and the secondary impact of (soil and vegetation) input parameter uncertainties. It is important to mention again that LSMs are continuously upgrading and that our study provides a relative comparison of older LSMs versions within LIS.

5.2 Effects of soil and vegetation parameters on soil moisture

Despite soil moisture being a highly model-dependent variable, it is important that soil moisture simulations closely mimic natural patterns to allow their use as underlying information in applications such as soil salinity monitoring over the Dry Chaco. Providing LSMs with the best available soil and vegetation parameters is one step towards this goal. The soil parameters strongly determine the spatial (horizontal and vertical) pattern of soil moisture (Figure 4), and only have a secondary impact on its temporal variability, which is mainly driven by meteorology. This was also reported by Morgan et al. (2017); Kishné et al. (2017); Zhao et al. (2018). The long-term soil moisture response to revised vegetation and land cover parameters differs among the three LSMs for two reasons:

– Soil moisture sensitivity to LAI and GVF indices ($SENS_V$): a decrease in LAI and GVF barely affects soil moisture in CLSM, whereas it increases soil moisture for CLM (moderately) and NOAH (strongly). This is in line with the respective LSM's degree of E_V extracting more or less water from the soil.

– Soil moisture sensitivity to land cover parameters ($SENS_{LC}$): a land cover change from forest to cropland barely affects CLM soil moisture, slightly increases soil moisture in CLSM, and mainly increases deep soil moisture in NOAH. This is related to the distinct root distribution and root water uptake (controlled by the stomatal conductance and rooting depth) in the various LSMs, impacting the E_V and related water extraction from the soil.

The REV_{SV} simulations showed that all three LSMs simulate wetter soils after deforestation in the Dry Chaco. In addition, larger values of total Q are found for two LSMs, which might implicitly be indicative of groundwater recharge (groundwater is only simulated in CLSM). This is in agreement with studies that have been carried out on a local scale by Giménez et al. (2016), Marchesini et al. (2017), Magliano et al. (2017) and Nosetto et al. (2012). They all reported wetter soils on agriculture land compared to forest across different regions of the Chaco. However, it must be mentioned that deforestation itself does not necessary lead to wetter soils. The impact of deforestation on soil moisture is a combination of an increased rate of E_B (drier soils) and a decreased rate of E_V (wetter soils). The net effect depends on the local climate and the length of the wet or dry periods (Chen et al., 2009). The impact may also vary across the vertical soil profile depending on the change in root distribution and soil characteristics after deforestation (de Queiroz et al., 2020). Amdan et al. (2013) stated that the agriculture system applied in north-west Argentina also influences the soil moisture status. The prevalent agriculture system in the Dry Chaco is mostly based on no-tillage management followed by fallow seasons. The crop residue that remains on the field decreases E_B and therefore increases available soil water content (Villegas et al., 2010). During the fallow season, there is no consumption of soil water over agriculture areas, increasing deep percolation of water towards the ground water table. These changes in soil characteristics, soil management and natural mulching are not included in LSM simulations.

5.3 Model evaluation using independent data

The reasonable agreement between MERRA-2 and the long-term in situ P data supports an analysis of the water budget components in absolute values (as in Table 2), but with caution: the more recent P stations suggest larger biases and may possibly not have been included in the gauge-based P corrections of MERRA-2. Due to its coarse resolution, MERRA-2 does not take into account microclimatic effects over the mosaic landscape associated with deforestation.

Relative to independent data, there is no LSM setup that yields significantly better output for the entire Dry Chaco in terms of time series metrics. CLM sfmc yields the largest R and aR values when compared to the in situ Monte Buey sfmc. NOAH outperforms both CLM and CLSM in terms of ET (when compared to GLEAM ET), whereas CLSM yields the best Tb results (when compared to SMOS Tb). Updating the model soil parameters with more recent (assumed to be more accurate) information reduces the sfmc bias relative to in situ observations for the 3 Monte Buey pixels, as well as the Tb bias relative to region-wide SMOS observations for all models. On the other hand, the update reduces the R values between CLSM and GLEAM ET and between CLSM and SMOS Tb.

The spatially complete time-series evaluation with long-term SMOS Tb observations is unique to assess model performance over areas with limited long-term in situ data. A similar approach was conducted by (Albergel et al., 2012) over the United States. The high R values between the SMOS Tb observations and RTM simulations indicate that LSMs simulate realistic temporal variations and that their use over the Dry Chaco is justified (despite the lower agreement between MERRA-2 and recent in situ P). After implementation of time-varying vegetation and land cover changes, we found no significant or unanimous model improvement when compared to independent data. This is most likely due to the coarse spatial resolution of the satellite-based evaluation, which suppresses the signal of the rather small-scale mosaic deforestation activities over the Chaco, and to the fact that model simulations do not necessarily perform better when given supposedly better input parameters. Furthermore, removal of subtropical dry forest is likely to only have a little impact on L-band Tb, whereas the removal of dense tropical rainforest would probably have a much stronger impact on both Tb simulations and observations. However, Figure 13 indicates that time-varying vegetation and land cover parameters did introduce slightly better agreements between simulated and SMOS-observed Tb for some deforested areas. Local calibration of different RTM parameters, could possibly further improve the agreements between modeled and observed Tb.

An evaluation with finer-scale sfmc retrievals e.g. obtained from Sentinel-1 or after downscaling passive microwave products, is not included in this study because by design, sfmc retrievals do not necessarily account well for deforestation, are prone to vegetation bias in general (Zwieback et al., 2018), and would thus not serve well as reference data. A finer-scale evaluation in terms of land surface temperature would add value, but an analysis of the energy budget was beyond the scope of this study.

5.4 Shortcomings and scope for further research

Our simulations of the Dry Chaco's hydrology with revised soil, vegetation and land cover parameters have some shortcomings and caveats that could partly be overcome in future research. First, feeding the models with similar, e.g. satellite-based, albedo input could further lead to a homogenization in model output as this is a key parameter in the calculation of land surface energy budget (Alton, 2009; Yin et al., 2016; Houspanossian et al., 2017). Second, we showed that the spatial pattern of simulated soil moisture is closely related to the spatial pattern of the soil texture data. Regional simulations could thus benefit from regional soil maps, where available. In addition, land cover changes can affect soil properties (Wiekenkamp et al., 2020), which means that the adjustment of SHPs in response to vegetation changes (such as deforestation) could further improve LSM simulations. Third, the relatively coarse spatial resolution of our simulations ($0.125°$) required an upscaling of the LAI, GVF and land cover input data, and the satellite-based evaluation even required an aggregation to 36 km. This caused a suppression of the deforestation signature in our simulations. Fourth, our LSM simulations did not include any dynamic vegetation growth module, which would couple soil moisture and vegetation two-ways, instead of only one-way. More generally, LSMs can benefit from further developments to better represent soil-water-vegetation processes, because the three tested LSMs now show a questionable range in their partitioning of the water budget components and in their response to parameter changes. Some of the above caveats will be addressed in future research towards using LSM output as underlying information for the assessment of dryland salinity over the Dry Chaco

6 Conclusions

In this study, we updated the soil- and vegetation-related parameters of three LSMs (CLM2.0, CLSM-F2.5 and Noah3.6), grouped within NASA's LIS, to obtain the best modeled representation of the hydrology over the South-American Dry Chaco. We used HWSD v1.21 soil texture and time-varying satellite-based GLASS and GIMMS vegetation indices, along with yearly updated ESA-CCI land cover information. The impact of the various model structures, soil texture and dynamic vegetation input was assessed in terms of water budget partitioning and efficiency space. Our results indicate that:

- the three LSMs yield a different partitioning of the water budget, with 74% to 95% of the total annual P over the Dry Chaco contributing to ET;
- the soil texture pattern is the main driver of the spatial pattern of soil moisture;
- introducing similar soil, vegetation and land cover parameters in the various LSMs does not result in a homogenization of the long-term water budget components, i.e. the various LSM structures primarily determine the water distribution whereas soil, vegetation and land cover parameters only have a secondary impact.

The updated vegetation and land cover treatment allowed to explore to which extent large-scale land cover changes in the Dry Chaco affect the different water budget components. It was found that:

- deforestation increases soil moisture for all LSMs, but the degree of increase is depending on the model structure;
- a change in land cover results in a shift of the model climatology and a (non-stationary) redistribution of the water budget, which is different for each LSM;
- the implemented satellite-based vegetation indices do not fully depict deforestation, because the $0.125°$ spatial resolution partially suppresses the deforestation signal, and the replacing agricultural crop may have similar LAI and GVF values as the initial dry forest.

The model input and output were further evaluated against independent data of in situ P and sfmc, and spatially covering GLEAM ET and SMOS Tb. The latter offers the unique possibility for an integral evaluation of simulated soil moisture, soil temperature and LAI, after forwarding these variables through a zero-order RTM. Relative to independent data, no specific LSM structure, soil or vegetation input is significantly better than another in terms of time series metrics. Updated soil parameters reduce Tb bias relative to region-wide SMOS observations for all models, improve the R and ubRMSD values for CLSM and NOAH, but reduce the R values between CLSM and GLEAM ET and CLSM and SMOS Tb. Interannually varying vegetation and land cover input generally has a marginal impact.

Our methodology is a first step towards a better representation of the Dry Chaco ecosystem using dynamic LSM simulations. The assimilation of multi-source remote sensing data for state (e.g. soil moisture and temperature) and parameter (e.g. albedo) updating may help to further constrain the models and correct for unmodelled processes, such as land cover changes. However, the impact of such updates will depend on the used LSM, and on the optimization of data assimilation systems in the presence of non-stationary processes that are associated with land cover changes (such as deforestation). Vegetation data assimilation can only have the desired impact, if the sensitivity of simulated hydrological fluxes to vegetation changes is realistic and this may need further research, especially at the global scale. To better represent small-scale land cover conversions and their impact on the water distribution for research on dryland salinity or ecology, simulations should also be conducted at a finer spatial resolution.

Author contributions. MM performed the model simulations, produced figures and wrote the paper; GDL and SA contributed to the experiment setup and the writing of the paper; SK and SP provided relevant input data for the simulations and contributed to the writing of the paper.

Competing interests. The authors declare that they have no conflict of interest.

Acknowledgements. This study was performed within the framework of the Belgian Science Policy (BELSPO) project REFORCHA (SR/00/338), with support of the Flemish Research Foundation (FWO 1512817N), C1 KU Leuven (C14/16/045) and using the High Performance Computing system of the Vlaams Supercomputer Centrum. The authors thank Mark Thibeault (CONAE) for providing the Monte Buey soil moisture data and David Mocko and Randy Koster for insightful discussions.

References

Albergel, C., Balsamo, G., Rosnay, P. d., Muñoz-Sabater, J., and Boussetta, S.: A bare ground evaporation revision in the ECMWF land-surface scheme: evaluation of its impact using ground soil moisture and satellite microwave data, Hydrology and Earth System Sciences, 16, 3607–3620, 2012.

Albergel, C., Munier, S., Leroux, D. J., Dewaele, H., Fairbairn, D., Barbu, A. L., Gelati, E., Dorigo, W., Faroux, S., Meurey, C., et al.: Sequential assimilation of satellite-derived vegetation and soil moisture products using SURFEX_v8.0: LDAS-Monde assessment over the Euro-Mediterranean area, Geoscientific Model Development, 10, 3889–3912, 2017.

Alton, P.: A simple retrieval of ground albedo and vegetation absorptance from MODIS satellite data for parameterisation of global land-surface models, Agricultural and Forest Meteorology, 149, 1769–1775, 2009.

Amdan, M., Aragón, R., Jobbágy, E., Volante, J., and Paruelo, J.: Onset of deep drainage and salt mobilization following forest clearing and cultivation in the Chaco plains (Argentina), Water Resources Research, 49, 6601–6612, 2013.

Balsamo, G., Beljaars, A., Scipal, K., Viterbo, P., van den Hurk, B., Hirschi, M., and Betts, A. K.: A revised hydrology for the ECMWF model: Verification from field site to terrestrial water storage and impact in the Integrated Forecast System, Journal of hydrometeorology, 10, 623–643, 2009.

Barbu, A. L., Calvet, J.-C., Mahfouf, J.-F., Albergel, C., and Lafont, S.: Assimilation of Soil Wetness Index and Leaf Area Index into the ISBA-A-gs land surface model: grassland case study, Biogeosciences, 8, 1971–1986, https://doi.org/10.5194/bg-8-1971-2011, https://bg.copernicus.org/articles/8/1971/2011/, 2011.

Barbu, A. L., Calvet, J.-C., Mahfouf, J.-F., and Lafont, S.: Integrating ASCAT surface soil moisture and GEOV1 leaf area index into the SURFEX modelling platform: a land data assimilation application over France, Hydrology and Earth System Sciences, 18, 173–192, https://doi.org/10.5194/hess-18-173-2014, https://hess.copernicus.org/articles/18/173/2014/, 2014.

Baret, F., Weiss, M., Lacaze, R., Camacho, F., Makhmara, H., Pacholcyzk, P., and Smets, B.: GEOV1: LAI and FAPAR essential climate variables and FCOVER global time series capitalizing over existing products. Part1: Principles of development and production, Remote sensing of environment, 137, 299–309, 2013.

Bonan, G. B., Levis, S., Kergoat, L., and Oleson, K. W.: Landscapes as patches of plant functional types: An integrating concept for climate and ecosystem models, Global Biogeochemical Cycles, 16, 5–1, 2002a.

Bonan, G. B., Oleson, K. W., Vertenstein, M., Levis, S., Zeng, X., Dai, Y., Dickinson, R. E., and Yang, Z.-L.: The land surface climatology of the Community Land Model coupled to the NCAR Community Climate Model, Journal of climate, 15, 3123–3149, 2002b.

Bontemps, S., Herold, M., Kooistra, L., Van Groenestijn, A., Hartley, A., Arino, O., Moreau, I., and Defourny, P.: Revisiting land cover observation to address the needs of the climate modeling community., Biogeosciences, 9, 2012.

Boussetta, S., Balsamo, G., Beljaars, A., Kral, T., and Jarlan, L.: Impact of a satellite-derived leaf area index monthly climatology in a global numerical weather prediction model, International journal of remote sensing, 34, 3520–3542, 2013.

Boussetta, S., Balsamo, G., Dutra, E., Beljaars, A., and Albergel, C.: Assimilation of surface albedo and vegetation states from satellite observations and their impact on numerical weather prediction, Remote Sensing of Environment, 163, 111–126, 2015.

Brocca, L., Tarpanelli, A., Filippucci, P., Dorigo, W., Zaussinger, F., Gruber, A., and Fernández-Prieto, D.: How much water is used for irrigation? A new approach exploiting coarse resolution satellite soil moisture products, International journal of applied earth observation and geoinformation, 73, 752–766, 2018.

Cao, Q., Yu, D., Georgescu, M., Han, Z., and Wu, J.: Impacts of land use and land cover change on regional climate: A case study in the agro-pastoral transitional zone of China, Environmental Research Letters, 10, 124 025, 2015.

Case, J. L., LaFontaine, F. J., Bell, J. R., Jedlovec, G. J., Kumar, S. V., and Peters-Lidard, C. D.: A real-time MODIS vegetation product for land surface and numerical weather prediction models, IEEE Transactions on Geoscience and Remote Sensing, 52, 1772–1786, 2013.

Chadburn, S., Burke, E., Essery, R., Boike, J., Langer, M., Heikenfeld, M., Cox, P. M., and Friedlingstein, P.: Impact of model developments on present and future simulations of permafrost in a global land-surface model, Cryosphere, pp. 1505–1521, 2015.

Chen, S., Su, H., and Zhan, J.: Estimating the impact of land use change on surface energy partition based on the Noah model, Frontiers of Earth Science, 8, 18–31, 2014.

Chen, X., Zhang, Z., Chen, X., and Shi, P.: The impact of land use and land cover changes on soil moisture and hydraulic conductivity along the karst hillslopes of southwest China, Environmental Earth Sciences, 59, 811–820, 2009.

Clark, M. L., Aide, T. M., Grau, H. R., and Riner, G.: A scalable approach to mapping annual land cover at 250 m using MODIS time series data: A case study in the Dry Chaco ecoregion of South America, Remote Sensing of Environment, 114, 2816–2832, 2010.

Clark, M. P., Fan, Y., Lawrence, D. M., Adam, J. C., Bolster, D., Gochis, D. J., Hooper, R. P., Kumar, M., Leung, L. R., Mackay, D. S., et al.: Improving the representation of hydrologic processes in Earth System Models, Water Resources Research, 51, 5929–5956, 2015.

Cosby, B., Hornberger, G., Clapp, R., and Ginn, T.: A statistical exploration of the relationships of soil moisture characteristics to the physical properties of soils, Water resources research, 20, 682–690, 1984.

Crawford, T. M., Stensrud, D. J., Mora, F., Merchant, J. W., and Wetzel, P. J.: Value of incorporating satellite-derived land cover data in MM5/PLACE for simulating surface temperatures, Journal of Hydrometeorology, 2, 453–468, 2001.

Csiszar, I. and Gutman, G.: Mapping global land surface albedo from NOAA AVHRR, Journal of Geophysical Research: Atmospheres, 104, 6215–6228, 1999.

Dai, Y., Shangguan, W., Wei, N., Xin, Q., Yuan, H., Zhang, S., Liu, S., Lu, X., Wang, D., and Yan, F.: A review of the global soil property maps for Earth system models, Soil, 5, 137–158, 2019.

De Lannoy, G. J., Reichle, R. H., and Pauwels, V. R.: Global calibration of the GEOS-5 L-band microwave radiative transfer model over nonfrozen land using SMOS observations, Journal of Hydrometeorology, 14, 765–785, 2013.

De Lannoy, G. J., Koster, R. D., Reichle, R. H., Mahanama, S. P., and Liu, Q.: An updated treatment of soil texture and associated hydraulic properties in a global land modeling system, Journal of Advances in Modeling Earth Systems, 6, 957–979, 2014.

De Lannoy, G. J., Reichle, R. H., Peng, J., Kerr, Y., Castro, R., Kim, E. J., and Liu, Q.: Converting between SMOS and SMAP level-1 brightness temperature observations over nonfrozen land, IEEE Geoscience and remote sensing letters, 12, 1908–1912, 2015.

de Queiroz, M. G., da Silva, T. G. F., Zolnier, S., Jardim, A. M. d. R. F., de Souza, C. A. A., Júnior, G. d. N. A., de Morais, J. E. F., and de Souza, L. S. B.: Spatial and temporal dynamics of soil moisture for surfaces with a change in land use in the semi-arid region of Brazil, CATENA, 188, 104 457, 2020.

Dickinson, R. E.: Land processes in climate models, Remote sensing of Environment, 51, 27–38, 1995.

Ducharne, A., Koster, R. D., Suarez, M. J., Stieglitz, M., and Kumar, P.: A catchment-based approach to modeling land surface processes in a general circulation model: 2. Parameter estimation and model demonstration, Journal of Geophysical Research: Atmospheres, 105, 24 823–24 838, 2000.

Ek, M., Mitchell, K., Lin, Y., Rogers, E., Grunmann, P., Koren, V., and Gayno, G.: Implementation of Noah Land Surface Model Advances in the National Centers for Environmental Prediction Operational Mesoscale Eta Model., Journal of Geophysical Research, 108, 8851, 2003.

Entekhabi, D., Reichle, R. H., Koster, R. D., and Crow, W. T.: Performance metrics for soil moisture retrievals and application requirements, Journal of Hydrometeorology, 11, 832–840, 2010.

ESA, L. C. C.: Product User Guide Version 2.0 (2017), Retrieved from: www. esa-landcovercci. org, 2017.

FAO, I. and ISRIC, I.: JRC: Harmonized World Soil Database (version 1.2), FAO, Rome, Italy and IIASA, Laxenburg, Austria, 2012.

FAO, U.: 1981. The FAO-Unesco Soil Map of the World. Legend and 9 volumes, 1971.

Feldman, A. F., Akbar, R., and Entekhabi, D.: Characterization of higher-order scattering from vegetation with SMAP measurements, Remote sensing of environment, 219, 324–338, 2018.

Ge, Q., Zhang, X., and Zheng, J.: Simulated effects of vegetation increase/decrease on temperature changes from 1982 to 2000 across the Eastern China, International Journal of Climatology, 34, 187–196, 2014.

Gelaro, R., McCarty, W., Suárez, M. J., Todling, R., Molod, A., Takacs, L., Randles, C. A., Darmenov, A., Bosilovich, M. G., Reichle, R., et al.: The modern-era retrospective analysis for research and applications, version 2 (MERRA-2), Journal of Climate, 30, 5419–5454, 2017.

Giménez, R., Mercau, J., Nosetto, M., Páez, R., and Jobbágy, E.: The ecohydrological imprint of deforestation in the semiarid Chaco: insights from the last forest remnants of a highly cultivated landscape, Hydrological Processes, 30, 2603–2616, 2016.

Girotto, M., De Lannoy, G. J., Reichle, R. H., Rodell, M., Draper, C., Bhanja, S. N., and Mukherjee, A.: Benefits and pitfalls of GRACE data assimilation: A case study of terrestrial water storage depletion in India, Geophysical research letters, 44, 4107–4115, 2017.

Grossman-Clarke, S., Zehnder, J. A., Loridan, T., and Grimmond, C. S. B.: Contribution of land use changes to near-surface air temperatures during recent summer extreme heat events in the Phoenix metropolitan area, Journal of Applied Meteorology and Climatology, 49, 1649–1664, 2010.

Gutman, G. and Ignatov, A.: The derivation of the green vegetation fraction from NOAA/AVHRR data for use in numerical weather prediction models, International Journal of remote sensing, 19, 1533–1543, 1998.

Han, X., Franssen, H.-J. H., Montzka, C., and Vereecken, H.: Soil moisture and soil properties estimation in the Community Land Model with synthetic brightness temperature observations, Water resources research, 50, 6081–6105, 2014.

Hansen, M. C., DeFries, R. S., Townshend, J. R., and Sohlberg, R.: Global land cover classification at 1 km spatial resolution using a classification tree approach, International journal of remote sensing, 21, 1331–1364, 2000.

Hansen, M. C., Potapov, P. V., Moore, R., Hancher, M., Turubanova, S. A., Tyukavina, A., Thau, D., Stehman, S., Goetz, S. J., Loveland, T. R., et al.: High-resolution global maps of 21st-century forest cover change, science, 342, 850–853, 2013.

Hengl, T., de Jesus, J. M., Heuvelink, G. B., Gonzalez, M. R., Kilibarda, M., Blagotić, A., Shangguan, W., Wright, M. N., Geng, X., Bauer-Marschallinger, B., et al.: SoilGrids250m: Global gridded soil information based on machine learning, PLoS one, 12, 2017.

Houspanossian, J., Giménez, R., Jobbágy, E., and Nosetto, M.: Surface albedo raise in the South American Chaco: Combined effects of deforestation and agricultural changes, Agricultural and Forest Meteorology, 232, 118–127, 2017.

INTA: Sistema De Información y Gestión Agrometeorológica, Instituto Nacional de Tecnologíca Agropecuaria, http://siga2.inta.gov.ar/#/, accessed 2020-01-15, 2020.

James, K. A., Stensrud, D. J., and Yussouf, N.: Value of real-time vegetation fraction to forecasts of severe convection in high-resolution models, Weather and Forecasting, 24, 187–210, 2009.

Jarlan, L., Balsamo, G., Lafont, S., Beljaars, A., Calvet, J.-C., and Mougin, E.: Analysis of leaf area index in the ECMWF land surface model and impact on latent heat and carbon fluxes: Application to West Africa, Journal of Geophysical Research: Atmospheres, 113, 2008.

Jiang, L., Kogan, F. N., Guo, W., Tarpley, J. D., Mitchell, K. E., Ek, M. B., Tian, Y., Zheng, W., Zou, C.-Z., and Ramsay, B. H.: Real-time weekly global green vegetation fraction derived from advanced very high resolution radiometer-based NOAA operational global vegetation index (GVI) system, Journal of Geophysical Research: Atmospheres, 115, 2010.

Jobbágy, E. G., Giménez, R., Marchesini, V., Diaz, Y., Jayawickreme, D. H., and Nosetto, M. D.: Salt Accumulation and Redistribution in the Dry Plains of Southern South America: Lessons from Land Use Changes, in: Saline and Alkaline Soils in Latin America, pp. 51–70, Springer, 2020.

Kaufmann, R. K., Zhou, L., Knyazikhin, Y., Shabanov, V., Myneni, R. B., and Tucker, C. J.: Effect of orbital drift and sensor changes on the time series of AVHRR vegetation index data, IEEE Transactions on Geoscience and Remote Sensing, 38, 2584–2597, 2000.

Kirches, G., Brockmann, C., Boettcher, M., Peters, M., Bontemps, S., Lamarche, C., Schlerf, M., Santoro, M., and Defourny, P.: Land Cover CCI-Product User Guide-Version 2, 2014.

Kishné, A. S., Yimam, Y. T., Morgan, C. L., and Dornblaser, B. C.: Evaluation and improvement of the default soil hydraulic parameters for the Noah Land Surface Model, Geoderma, 285, 247–259, 2017.

Knyazikhin, Y., Martonchik, J., Myneni, R. B., Diner, D., and Running, S. W.: Synergistic algorithm for estimating vegetation canopy leaf area index and fraction of absorbed photosynthetically active radiation from MODIS and MISR data, Journal of Geophysical Research: Atmospheres, 103, 32 257–32 275, 1998.

Koster, R.: "Efficiency space": A framework for evaluating joint evaporation and runoff behavior, Bulletin of the American Meteorological Society, 96, 393–396, 2015.

Koster, R. D., Suarez, M. J., Ducharne, A., Stieglitz, M., and Kumar, P.: A catchment-based approach to modeling land surface processes in a general circulation model: 1. Model structure, Journal of Geophysical Research: Atmospheres, 105, 24 809–24 822, 2000.

Koster, R. D., Guo, Z., Yang, R., Dirmeyer, P. A., Mitchell, K., and Puma, M. J.: On the nature of soil moisture in land surface models, Journal of Climate, 22, 4322–4335, 2009.

Koster, R. D., Mahanama, P., and P, S.: Land surface controls on hydroclimatic means and variability, Journal of Hydrometeorology, 13, 1604–1620, 2012.

Kumar, A., Chen, F., Barlage, M., Ek, M. B., and Niyogi, D.: Assessing impacts of integrating MODIS vegetation data in the weather research and forecasting (WRF) model coupled to two different canopy-resistance approaches, Journal of Applied Meteorology and Climatology, 53, 1362–1380, 2014.

Kumar, S., Holmes, T., Mocko, D., Wang, S., and Peters-Lidard, C.: Attribution of flux partitioning variations between land surface models over the continental us, Remote Sensing, 10, 751, 2018.

Kumar, S. V., Peters-Lidard, C. D., Tian, Y., Houser, P. R., Geiger, J., Olden, S., Lighty, L., Eastman, J. L., Doty, B., Dirmeyer, P., et al.: Land information system: An interoperable framework for high resolution land surface modeling, Environmental modelling & software, 21, 1402–1415, 2006.

Kumar, S. V., Peters-Lidard, C. D., Eastman, J. L., and Tao, W.-K.: An integrated high-resolution hydrometeorological modeling testbed using LIS and WRF, Environmental Modelling & Software, 23, 169–181, 2008.

Kumar, S. V., Peters-Lidard, C. D., Santanello, J. A., Reichle, R. H., Draper, C. S., Koster, R. D., Nearing, G., and Jasinski, M. F.: Evaluating the utility of satellite soil moisture retrievals over irrigated areas and the ability of land data assimilation methods to correct for unmodeled processes, Hydrology and Earth System Sciences, 19, 4463–4478, https://doaj.org/article/100ac202879e4c2e81e1d5087be18413, 2015.

Kumar, S. V., M. Mocko, D., Wang, S., Peters-Lidard, C. D., and Borak, J.: Assimilation of Remotely Sensed Leaf Area Index into the Noah-MP Land Surface Model: Impacts on Water and Carbon Fluxes and States over the Continental United States, Journal of Hydrometeorology, 20, 1359–1377, 2019.

Lawrence, D. M., Thornton, P. E., Oleson, K. W., and Bonan, G. B.: The partitioning of evapotranspiration into transpiration, soil evaporation, and canopy evaporation in a GCM: Impacts on land–atmosphere interaction, Journal of Hydrometeorology, 8, 862–880, 2007.

Liang, S., Zhao, X., Liu, S., Yuan, W., Cheng, X., Xiao, Z., Zhang, X., Liu, Q., Cheng, J., Tang, H., et al.: A long-term Global LAnd Surface Satellite (GLASS) data-set for environmental studies, International Journal of Digital Earth, 6, 5–33, 2013.

Magliano, P. N., Fernández, R. J., Florio, E. L., Murray, F., and Jobbágy, E. G.: Soil physical changes after conversion of woodlands to pastures in Dry Chaco Rangelands (Argentina), Rangeland Ecology & Management, 70, 225–229, 2017.

Marchesini, V. A., Giménez, R., Nosetto, M. D., and Jobbágy, E. G.: Ecohydrological transformation in the Dry Chaco and the risk of dryland salinity: Following Australia's footsteps?, Ecohydrology, 10, e1822, 2017.

Marchesini, V. A., Nosetto, M. D., Houspanossian, J., and Jobbágy, E. G.: Contrasting hydrological seasonality with latitude in the South American Chaco: The roles of climate and vegetation activity, Journal of Hydrology, 587, 124 933, 2020.

Martens, B., Gonzalez Miralles, D., Lievens, H., Van Der Schalie, R., De Jeu, R. A., Fernández-Prieto, D., Beck, H. E., Dorigo, W., and Verhoest, N.: GLEAM v3: Satellite-based land evaporation and root-zone soil moisture, Geoscientific Model Development, 10, 1903–1925, 2017.

Miller, J., Barlage, M., Zeng, X., Wei, H., Mitchell, K., and Tarpley, D.: Sensitivity of the NCEP/Noah land surface model to the MODIS green vegetation fraction data set, Geophysical research letters, 33, 2006.

Minetti, J. L., Albarracín, S. A., Bobba, M. E., Hernández, C. M., López, E. R., Acuña, L. A., Costa, M. C., Nieva, I. J., and Mendoza, E.: Atlas climático del noroeste argentino, 1999.

Miralles, D. G., Holmes, T., De Jeu, R., Gash, J., Meesters, A., and Dolman, A.: Global land-surface evaporation estimated from satellite-based observations, Hydrology and Earth System Sciences, pp. 453–469, 2011.

Morgan, C. L., Yimam, Y. T., Barlage, M., Gochis, D., and Dornblaser, B.: Valuing of soil capability in land surface modeling, in: Global Soil Security, pp. 53–61, Springer, 2017.

Nosetto, M. D., Jobbágy, E., Brizuela, A. B., and Jackson, R.: The hydrologic consequences of land cover change in central Argentina, Agriculture, Ecosystems & Environment, 154, 2–11, 2012.

Oleson, K., Dai, Y., Bonan, G., Bosilovich, M., Dickinson, R., Dirmeyer, P., Hoffman, F., Houser, P., Levis, S., Niu, G., et al.: Technical description of the community land model (CLM), NCAR Technical Note, 2004.

Oleson, K. W., Bonan, G. B., Schaaf, C., Gao, F., Jin, Y., and Strahler, A.: Assessment of global climate model land surface albedo using MODIS data, Geophysical Research Letters, 30, 2003.

O'Neill, P., Njoku, E., Jackson, T., Chan, S., and Bindlish, R.: SMAP algorithm theoretical basis document: Level 2 & 3 soil moisture (passive) data products, Jet Propulsion Lab., California Inst. Technol., Pasadena, CA, USA, JPL D-66480, 2015.

Peters-Lidard, C. D., Houser, P. R., Tian, Y., Kumar, S. V., Geiger, J., Olden, S., Lighty, L., Doty, B., Dirmeyer, P., Adams, J., et al.: High-performance Earth system modeling with NASA/GSFC's Land Information System, Innovations in Systems and Software Engineering, 3, 157–165, 2007.

Pinzon, J. E. and Tucker, C. J.: A non-stationary 1981–2012 AVHRR NDVI3g time series, Remote sensing, 6, 6929–6960, 2014.

Pitman, A. J.: The evolution of, and revolution in, land surface schemes designed for climate models, International Journal of Climatology: A Journal of the Royal Meteorological Society, 23, 479–510, 2003.

Pitman, A. J., de Noblet-Ducoudré, N., Cruz, F., Davin, E. L., Bonan, G., Brovkin, V., Claussen, M., Delire, C., Ganzeveld, L., Gayler, V., et al.: Uncertainties in climate responses to past land cover change: First results from the LUCID intercomparison study, Geophysical Research Letters, 36, 2009.

Priestley, C. H. B. and Taylor, R.: On the assessment of surface heat flux and evaporation using large-scale parameters, Monthly weather review, 100, 81–92, 1972.

Quets, J., De Lannoy, G. J., Al Yaari, A., Chan, S., Cosh, M. H., Gruber, A., Reichle, R. H., Van der Schalie, R., and Wigneron, J.-P.: Uncertainty in soil moisture retrievals: An ensemble approach using SMOS L-band microwave data, Remote sensing of environment, 229, 133–147, 2019.

Reichle, R. H., Koster, R. D., De Lannoy, G. J., Forman, B. A., Liu, Q., Mahanama, S. P., and Touré, A.: Assessment and enhancement of MERRA land surface hydrology estimates, Journal of climate, 24, 6322–6338, 2011.

Reichle, R. H., Draper, C. S., Liu, Q., Girotto, M., Mahanama, S. P., Koster, R. D., and De Lannoy, G. J.: Assessment of MERRA-2 land surface hydrology estimates, Journal of Climate, 30, 2937–2960, 2017.

Reichle, R. H., Liu, Q., Koster, R. D., Crow, W. T., De Lannoy, G. J., Kimball, J. S., Ardizzone, J. V., Bosch, D., Colliander, A., Cosh, M., et al.: Version 4 of the SMAP Level-4 Soil Moisture Algorithm and Data Product, Journal of Advances in Modeling Earth Systems, 11, 3106–3130, 2019.

Rigden, A. J., Salvucci, G. D., Entekhabi, D., and Short Gianotti, D. J.: Partitioning evapotranspiration over the continental United States using weather station data, Geophysical Research Letters, 45, 9605–9613, 2018.

Ruiz-Vasquez, M., Arias, P. A., Martínez, J. A., and Espinoza, J. C.: Effects of Amazon basin deforestation on regional atmospheric circulation and water vapor transport towards tropical South America, Climate Dynamics, pp. 1–21, 2020.

Sabater, J. M., Rüdiger, C., Calvet, J.-C., Fritz, N., Jarlan, L., and Kerr, Y.: Joint assimilation of surface soil moisture and LAI observations into a land surface model, Agricultural and Forest Meteorology, 148, 1362–1373, 2008.

Sellers, P., Mintz, Y., Sud, Y. e. a., and Dalcher, A.: A simple biosphere model (SiB) for use within general circulation models, Journal of the Atmospheric Sciences, 43, 505–531, 1986.

Thibeault, M., Cáceres, J. M., Dadamia, D., Soldano, A. G., Quirno, M. U., Guerrieri, J. M., Edrosa, R., Palomeque, M., Romaldi, L., Pucheta, J., et al.: Spatial and temporal analysis of the Monte Buey SAOCOM and SMAP core site., in: IEEE International Geoscience and Remote Sensing Symposium (IGARSS), pp. 969–971, IEEE, 2015.

Tucker, C. J., Pinzon, J. E., Brown, M. E., Slayback, D. A., Pak, E. W., Mahoney, R., Vermote, E. F., and El Saleous, N.: An extended AVHRR 8-km NDVI dataset compatible with MODIS and SPOT vegetation NDVI data, International Journal of Remote Sensing, 26, 4485–4498, 2005.

Vallejos, M., Volante, J. N., Mosciaro, M. J., Vale, L. M., Bustamante, M. L., and Paruelo, J. M.: Transformation dynamics of the natural cover in the Dry Chaco ecoregion: a plot level geo-database from 1976 to 2012, Journal of Arid Environments, 123, 3–11, 2015.

Villegas, J. C., Breshears, D. D., Zou, C. B., and Law, D. J.: Ecohydrological controls of soil evaporation in deciduous drylands: how the hierarchical effects of litter, patch and vegetation mosaic cover interact with phenology and season, Journal of Arid Environments, 74, 595–602, 2010.

Wang, J. R. and Schmugge, T. J.: An Empirical Model for the Complex Dielectric Permittivity of Soils as a Function of Water Content, IEEE Transactions on Geoscience and Remote Sensing, GE-18, 288–295, 1980.

Wang, K. and Dickinson, R. E.: A review of global terrestrial evapotranspiration: Observation, modeling, climatology, and climatic variability, Reviews of Geophysics, 50, 2012.

Wei, H., Xia, Y., Mitchell, K. E., and Ek, M. B.: Improvement of the Noah land surface model for warm season processes: Evaluation of water and energy flux simulation, Hydrological Processes, 27, 297–303, 2013.

Wiekenkamp, I., Huisman, J. A., Bogena, H. R., and Vereecken, H.: Effects of Deforestation on Water Flow in the Vadose Zone, Water, 12, 35, 2020.

Wood, E. F., Roundy, J. K., Troy, T. J., Van Beek, L., Bierkens, M. F., Blyth, E., de Roo, A., Döll, P., Ek, M., Famiglietti, J., et al.: Hyperresolution global land surface modeling: Meeting a grand challenge for monitoring Earth's terrestrial water, Water Resources Research, 47, 2011.

Wösten, J., Lilly, A., Nemes, A., and Le Bas, C.: Development and use of a database of hydraulic properties of European soils, Geoderma, 90, 169–185, 1999.

Wösten, J., Pachepsky, Y. A., and Rawls, W.: Pedotransfer functions: bridging the gap between available basic soil data and missing soil hydraulic characteristics, Journal of hydrology, 251, 123–150, 2001.

Xiao, Z., Liang, S., Wang, J., Xiang, Y., Zhao, X., and Song, J.: Long-time-series global land surface satellite leaf area index product derived from MODIS and AVHRR surface reflectance, IEEE Transactions on Geoscience and Remote Sensing, 54, 5301–5318, 2016.

Yin, J., Zhan, X., Zheng, Y., Hain, C. R., Ek, M., Wen, J., Fang, L., and Liu, J.: Improving Noah land surface model performance using near real time surface albedo and green vegetation fraction, Agricultural and forest meteorology, 218, 171–183, 2016.

Zeng, X.: Global vegetation root distribution for land modeling, Journal of Hydrometeorology, 2, 525–530, 2001.

Zhang, B., Xia, Y., Long, B., Hobbins, M., Zhao, X., Hain, C., Li, Y., and Anderson, M. C.: Evaluation and comparison of multiple evapotranspiration data models over the contiguous United States: Implications for the next phase of NLDAS (NLDAS-Testbed) development, Agricultural and Forest Meteorology, 280, 107 810, 2020.

Zhao, H., Zeng, Y., Lv, S., and Su, Z.: Analysis of soil hydraulic and thermal properties for land surface modeling over the Tibetan Plateau, Earth system science data, 10, 1031, 2018.

Zhu, Z., Bi, J., Pan, Y., Ganguly, S., Anav, A., Xu, L., Samanta, A., Piao, S., Nemani, R., and Myneni, R.: Global data sets of vegetation leaf area index (LAI) 3g and fraction of photosynthetically active radiation (FPAR) 3g derived from global inventory modeling and mapping studies (GIMMS) normalized difference vegetation index (NDVI3g) for the period 1981 to 2011, Remote sensing, 5, 927–948, 2013.

Zwieback, S., Colliander, A., Cosh, M. H., Martínez-Fernández, J., McNairn, H., Starks, P. J., Thibeault, M., and Berg, A.: Estimating time-dependent vegetation biases in the SMAP soil moisture product, Hydrology and Earth System Sciences, 22, 4473–4489, 2018.

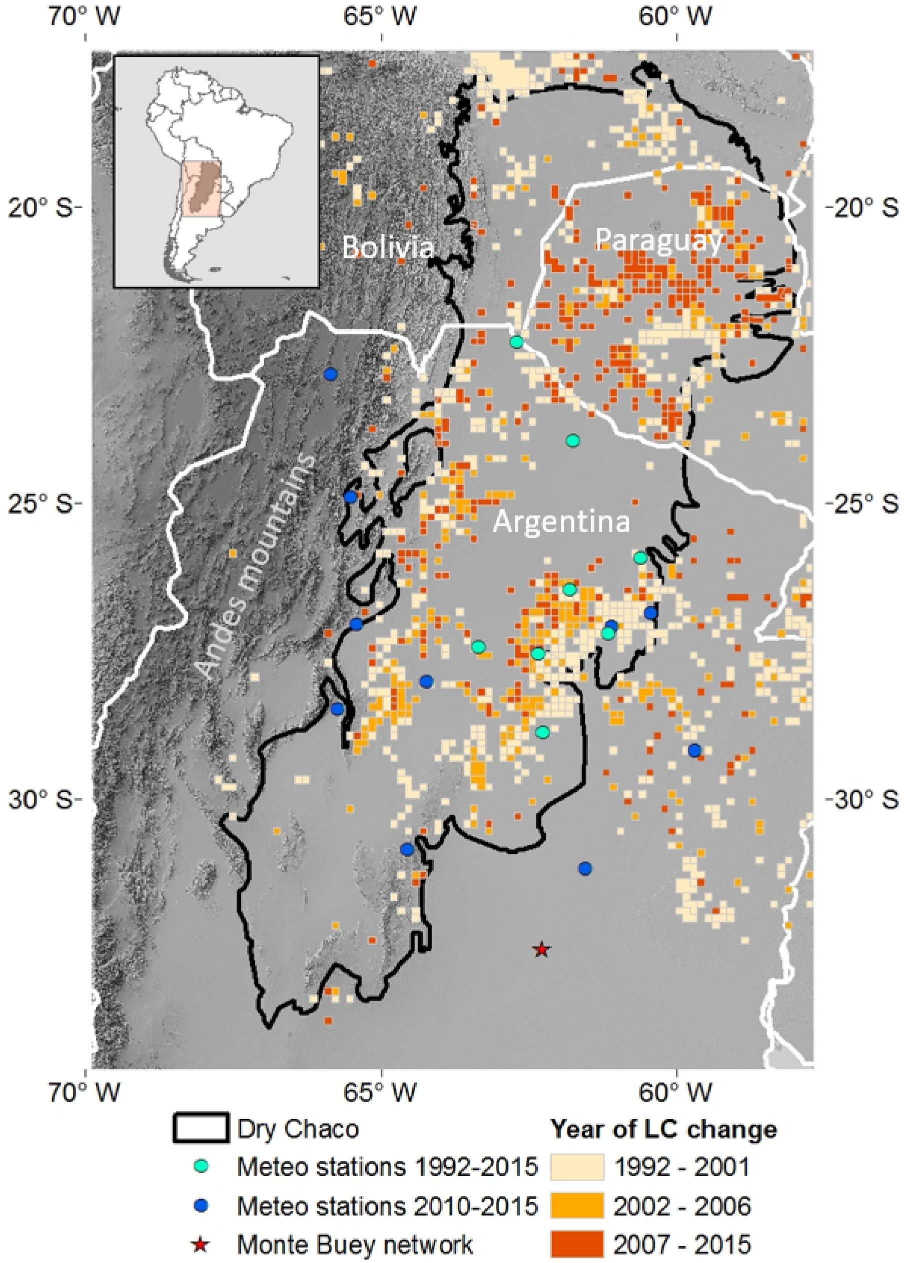

Figure 1. Geographic location of the Dry Chaco ecoregion together with the spatio-temporal pattern of land cover (LC) changes obtained from the ESA-CCI land cover product (upscaled to 0.125° resolution) together with the location of the Monte Buey soil moisture site and in situ meteorological stations used for validation of soil moisture and precipitation, respectively.

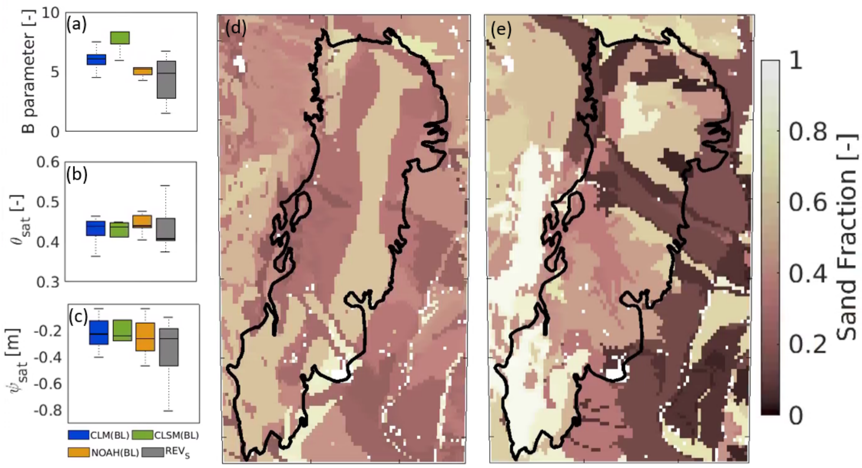

Figure 2. Spatial boxplots of soil parameters: (a) B parameter, (b) porosity θ_{sat} and (c) saturated matric potential ψ_{sat} used in BL and REV_S simulations. Sand fraction maps associated with (d) BL (FAO surface texture), and (e) REV_S and REV_{SV} (HWSDv1.21 0-100 cm texture).

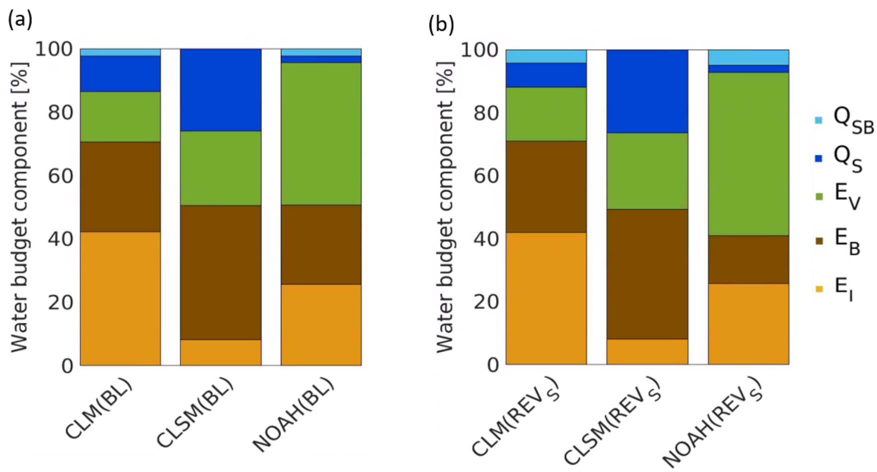

Figure 3. Long-term (1992-2015) annual water budget components averaged over the Dry Chaco, relative to the total precipitation for (a) BL and (b) REV_S experiments (Q_{SB}: Subsurface runoff, Q_S: Surface runoff, E_V: Vegetation transpiration, E_B: Bare soil evaporation, E_I: Interception evaporation).

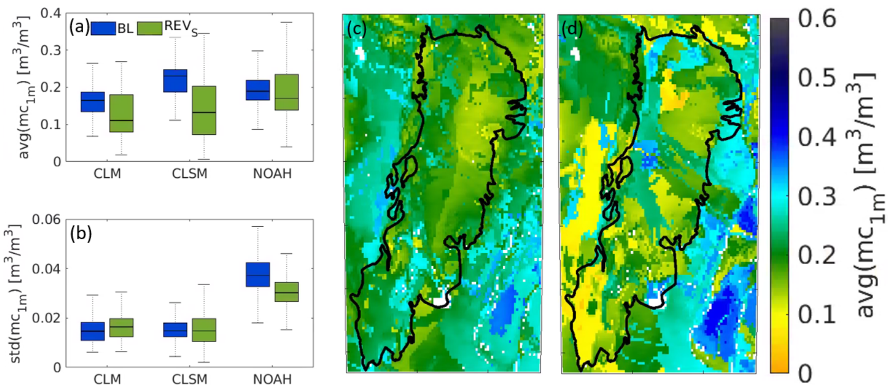

Figure 4. Boxplots of long-term (1992-2015) (a) average (avg) and (b) standard deviation (std) of BL and REV_S moisture content in the upper 1 m (mc_{1m}) for CLM, CLSM and NOAH. Maps of long-term (1992-2015) average NOAH mc_{1m}, obtained with (c) BL and (d) REV_S parameters.

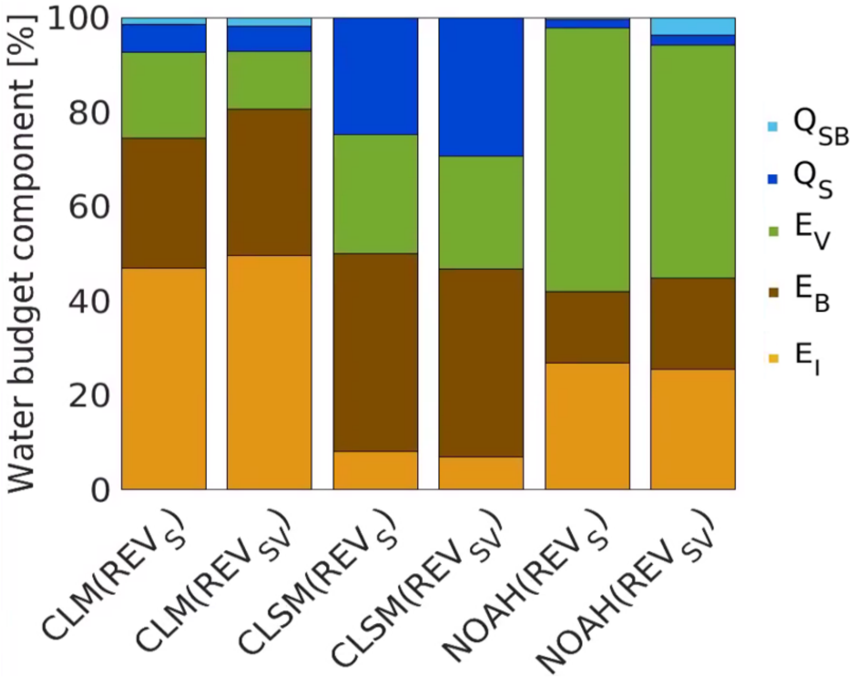

Figure 5. Annual water budget components for the period 2007-2015 relative to the total precipitation for the 197 pixels deforested between 2002 and 2006 for REV_S and REV_{SV} simulations (Q_{SB}: Subsurface runoff, Q_S: Surface runoff, E_V: Vegetation transpiration, E_B: Bare soil evaporation, E_I: Interception evaporation).

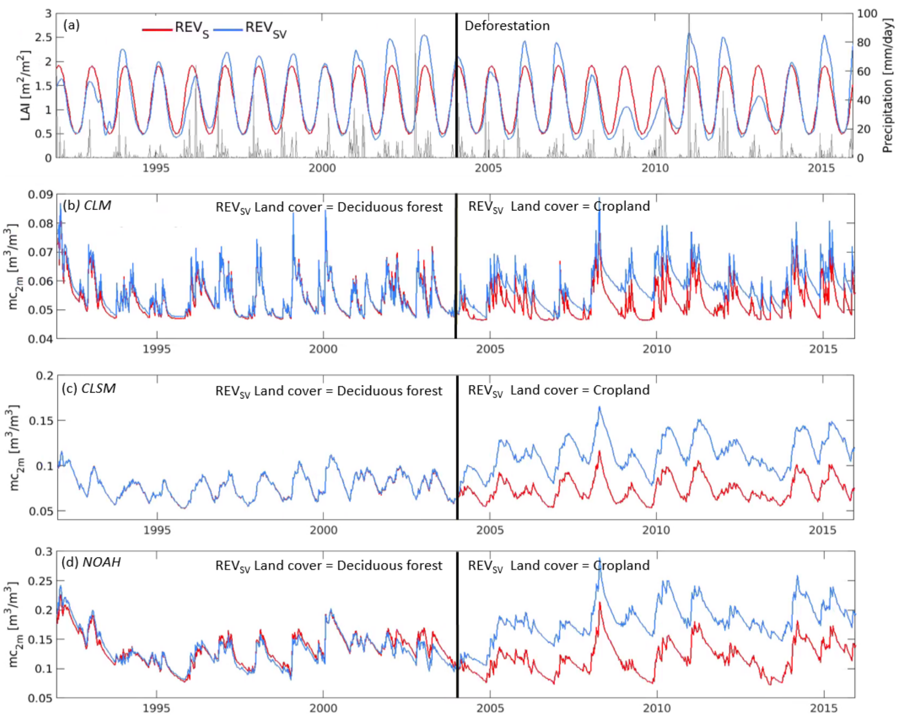

Figure 6. Time series of REV_S and REV_{SV} land surface variables for a pixel deforested in 2004 (28.0625° S, 63.6875° W): (a) LAI and precipitation, (b-c-d) 2 m moisture content (mc_{2m}) for CLM, CLSM and NOAH, respectively.

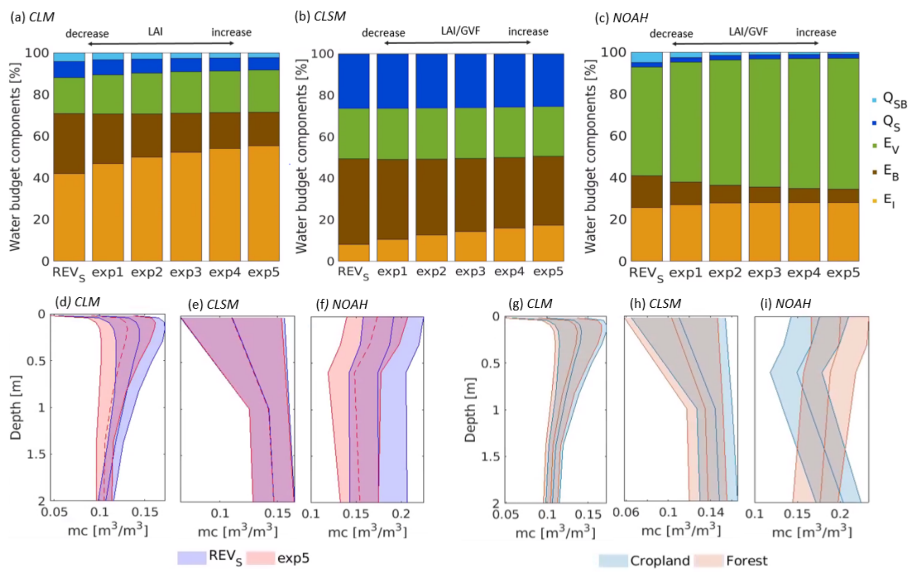

Figure 7. (a-b-c) Long-term (1992-2015) water budget components averaged over the Dry Chaco for $SENS_V$ experiments, for CLM, CLSM and NOAH, respectively. Exp1 to exp5 refer to simulations whereby the monthly climatological LAI maps were increased with respectively 1 to 5 units (Q_{SB}: Subsurface runoff, Q_S: Surface runoff, E_V: Vegetation transpiration, E_B: Bare soil evaporation, E_I: Interception evaporation). (d-e-f) Associated impact on the soil moisture profile (spatially averaged profile) for CLM, CLSM and NOAH, respectively. (g-h-i) Impact of changing land cover parameters ($SENS_{LC}$) from deciduous forest to cropland on the soil moisture profile for CLM, CLSM and NOAH, respectively.

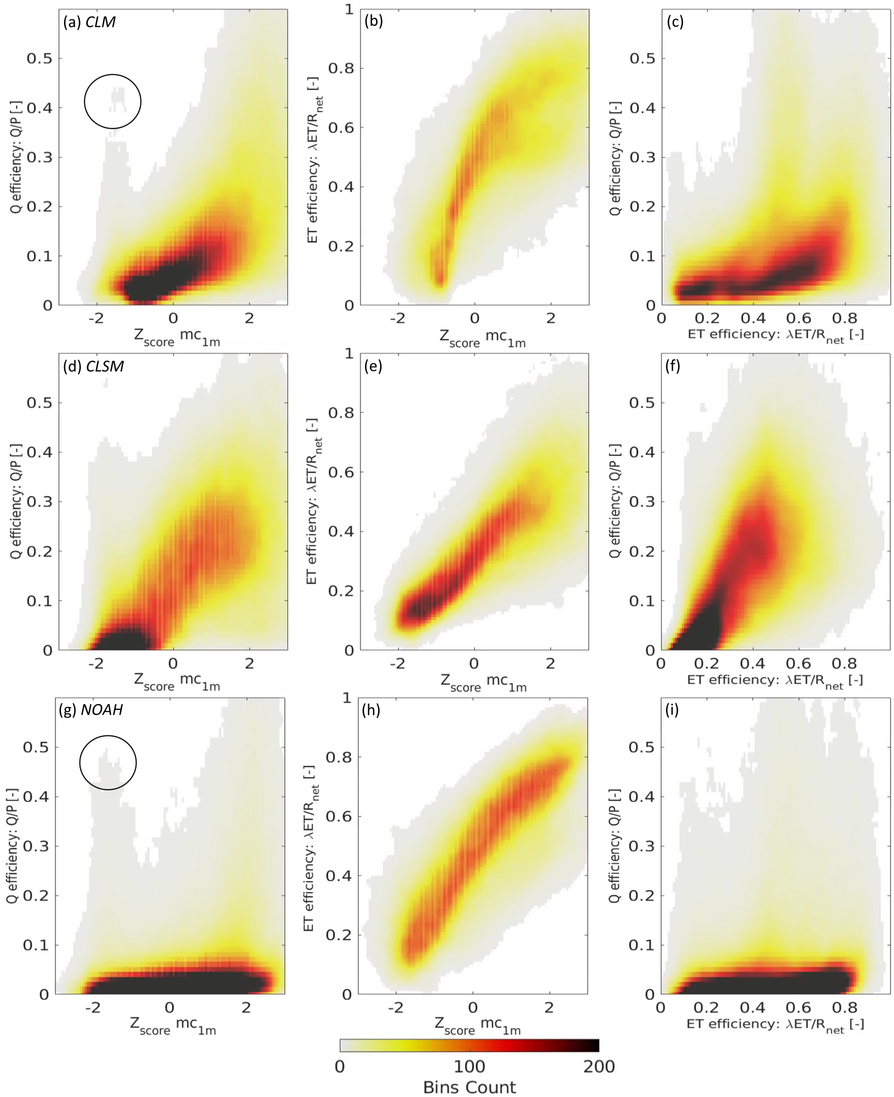

Figure 8. Scatter density clouds representing the fitted curves in efficiency space of all pixels inside the Dry Chaco for the BL experiment for the period 1992-2015 for (a-b-c) CLM, (d-e-f) CLSM and (g-h-i) NOAH, respectively. (Left) Q efficiency, (middle) ET efficiency and (right) ET vs Q efficiency.

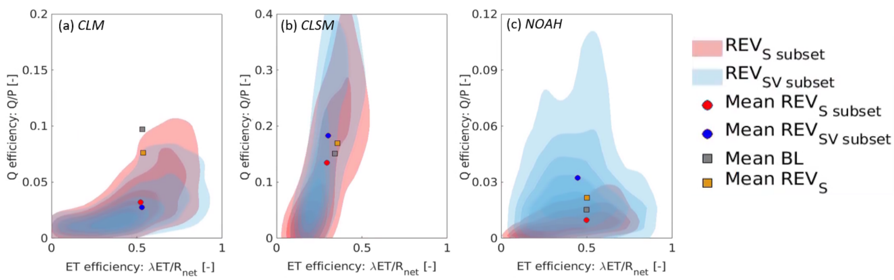

Figure 9. Scatter clouds in efficiency space for the REV_S (red) and REV_{SV} (blue) experiment for a subset of 197 pixels (corresponding with deforested pixels between 2002-2006) for the period 2007-2015, together with the mean value for (a-b-c) CLM, CLSM and NOAH, respectively. The gray and orange dots represent the shift in mean efficiency between the BL and REV_S simulations, based on all pixels inside the Dry Chaco, i.e. the mean BL values correspond to those in Figure 8 (c-f-i).

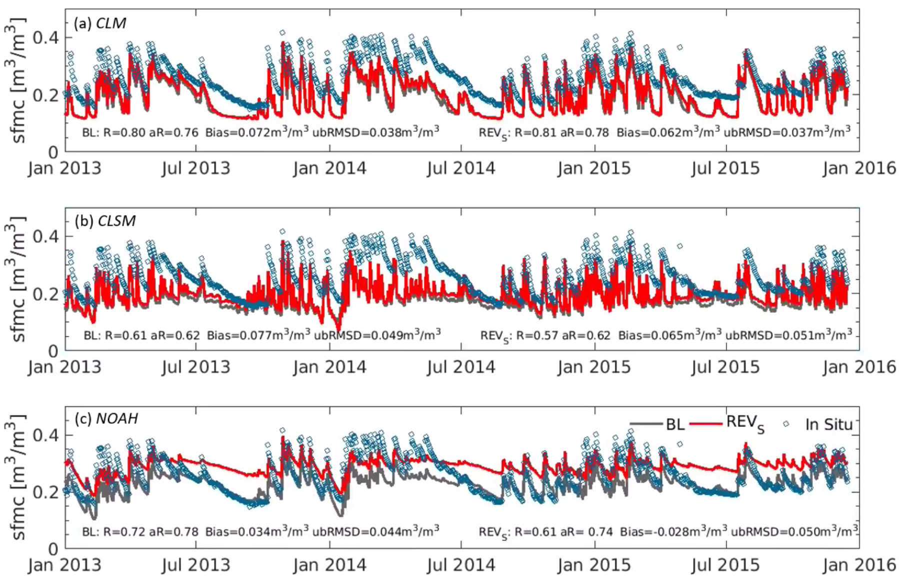

Figure 10. Simulated (BL and REV_S) and in situ observed surface soil moisture (sfmc) time series at Monte Buey, Argentina (32.91° S, 62.44° W), for the period January 2013-December 2015, for (a-b-c) CLM, CLSM and NOAH, respectively.

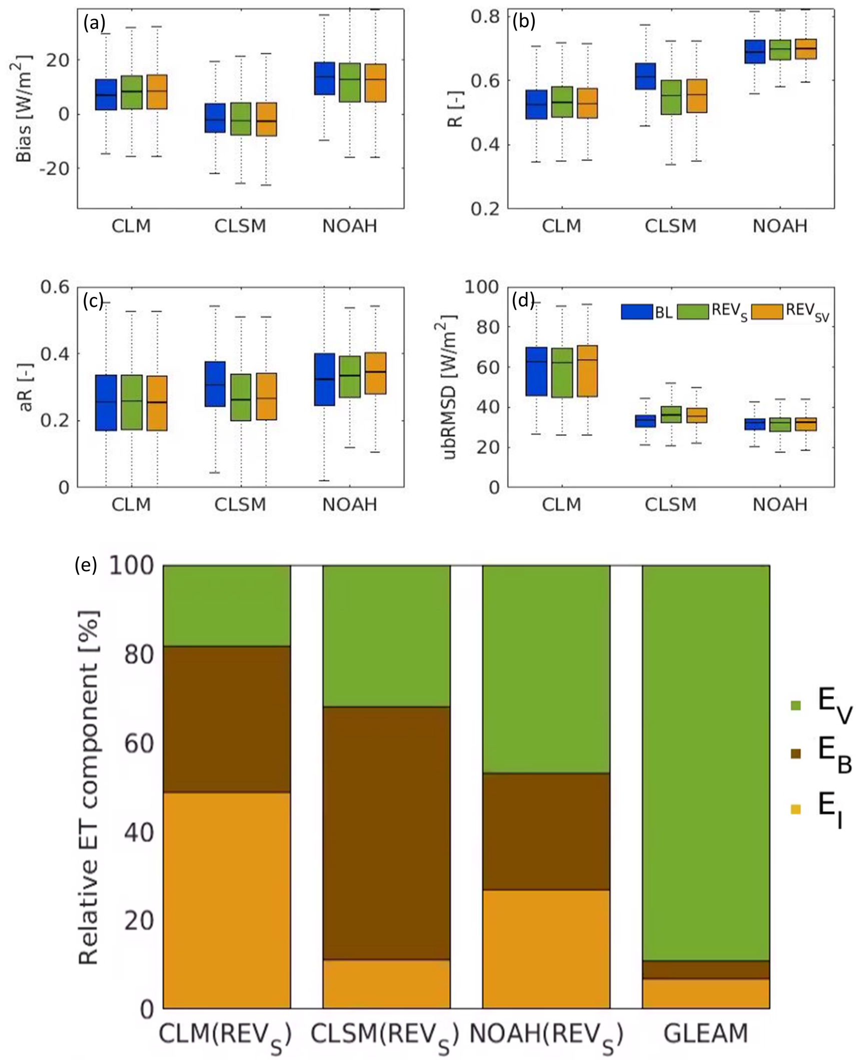

Figure 11. (a-d) Skill metrics for total ET from CLM, CLSM, NOAH (BL, REV_SV and REV_{SV}) relative to GLEAM, calculated for the period 1992-2015 over all pixels inside the Dry Chaco. (e) Long-term (1992-2015) relative ET components (E_V: Vegetation transpiration, E_B: Bare soil evaporation, E_I: Interception evaporation) spatially averaged over the Dry Chaco for REV_S CLM, CLSM, NOAH and GLEAM.

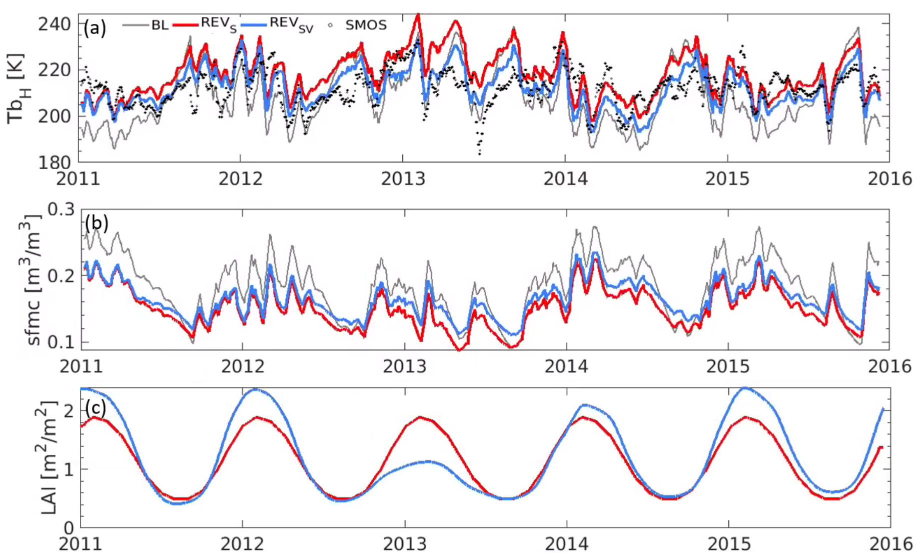

Figure 12. Time series of simulated (gray) BL, (red) REV_S, (blue) REV_{SV} NOAH-based (a) Tb$_H$, (b) sfmc and (c) LAI input at the same location as in Figure 6, but upscaled to the 36-km EASEv2-grid resolution. Also shown are (black dots) SMOS observed Tb$_H$ in subplot (a).

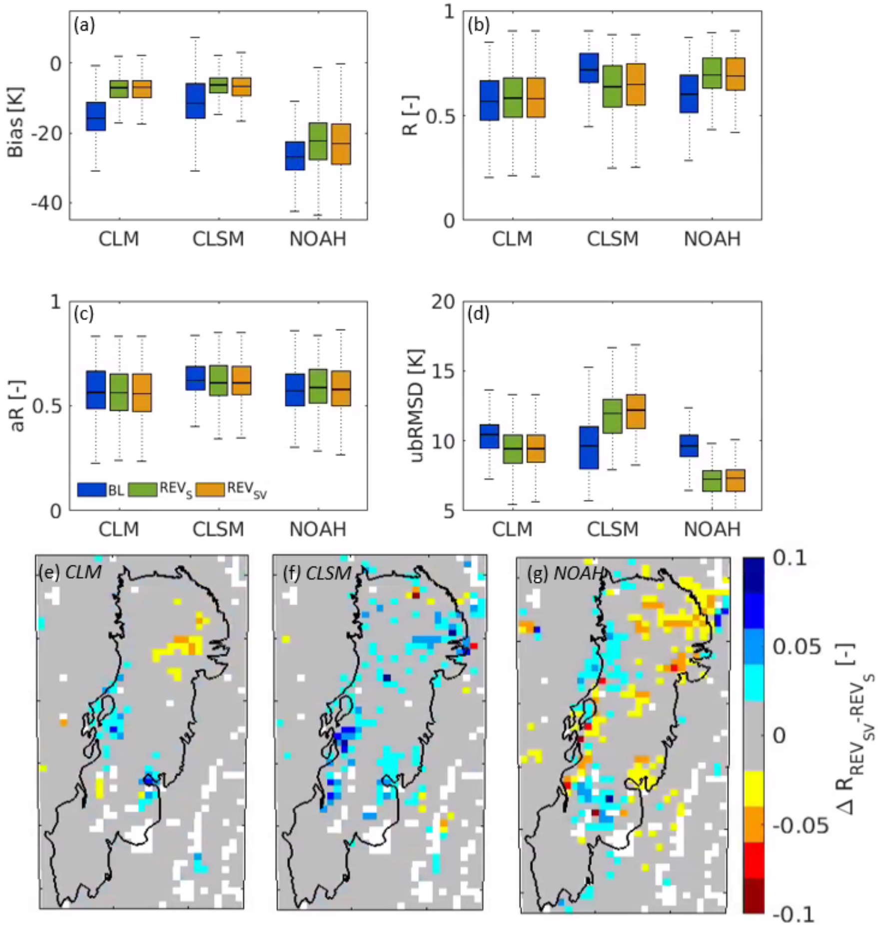

Figure 13. (a-d) Skill metrics for CLM, CLSM, NOAH (BL, REV_{SV} and REV_{SV}) Tb relative to SMOS Tb, calculated for the period 2011-2015 over pixels deforested between 2002 and 2006. (e-f-g) difference between the R metric for REV_{SV} and REV_S for CLM, CLSM and NOAH, respectively.

Tables

Table 1. Overview of experiments.

Name	Soil data	Vegetation	Land Cover
BL	FAO	climatology	ESA-CCI 1992
REV_S	HWSD	climatology	ESA-CCI 1992
REV_{SV}	HWSD	time-varying	ESA-CCI yearly updated
$SENS_V$	HWSD	increasing climatology	ESA-CCI 1992
$SENS_{LC}$	HWSD	climatology	forest or agriculture

Table 2. Long-term (1992-2015) distribution of the BL water budget components [mm] for CLM, CLSM and NOAH over the Dry Chaco, year-round (Annual), for the months April-September (Dry season) and the months October-March (Wet season), respectively.

	CLM			CLSM			NOAH		
	Annual	Dry	Wet	Annual	Dry	Wet	Annual	Dry	Wet
P	809	166	643	809	166	643	809	166	643
ET	698	162	536	599	172	427	773	221	552
Q_S	91	16	75	210	35	175	18	3	15
Q_{SB}	20	6	14	0	0	0	18	8	10
ΔS	0	-18	18	0	-41	41	0	-66	66

Table 3. Skill metrics for monthly MERRA-2 relative to in situ precipitation: spatial average ± spatial standard deviation.

	Bias [mm/month]	ubRMSD [mm/month]	R [-]
$\text{Stations}_{\text{1992-2015}}$ (n=10)	5 ± 11	38 ± 17	0.83 ± 0.07
$\text{Stations}_{\text{2010-2015}}$ (n=8)	18 ± 13	42 ± 14	0.74 ± 0.11

Table A1. Conversion from the ESA-CCI to the UMD land cover classification

ESA CCI	UMD
No data	No data
Cropland, rainfed	Cropland
Cropland, herbaceous cover	Cropland
Cropland, tree or shrub cover	Cropland
Cropland, irrigated or post-flooding	Cropland
Mosaic cropland (>50%) natural vegetation (tree, shrub, herbaceous cover) (<50%)	Cropland
Mosaic natural vegetation (tree, shrub, herbaceous cover) (>50%), cropland (<50%)	Open shrubland
Tree cover, broadleaved, evergreen, closed to open (>15%)	Evergreen broadleaf forest
Tree cover, broadleaved, deciduous, closed to open (>15%)	Deciduous broadleaf forest
Tree cover, broadleaved, deciduous, closed (>40%)	Deciduous broadleaf forest
Tree cover, broadleaved, deciduous, open (15-40%)	Deciduous broadleaf forest
Tree cover, needleleaved, evergreen, closed to open (>15%)	Evergreen needleleaf forest
Tree cover, needleleaved, evergreen, closed (>40%)	Evergreen needleleaf forest
Tree cover, needleleaved, evergreen, open (15-40%))	Evergreen needleleaf forest
Tree cover, needleleaved, deciduous, closed to open (>15%)	Deciduous needleleaf forest
Tree cover, needleleaved, deciduous, closed (>40%)	Deciduous needleleaf forest
Tree cover, needleleaved, deciduous, open (15-40%)	Deciduous needleleaf forest
Tree cover, mixed leaf type (broadleaved and needleleaved)	Mixed cover
Mosaic tree and shrub (>50%), herbaceous cover (<50%)	Woodland
Mosaic herbaceous cover (>50%), tree and shrub (<50%)	Woodland
Shrubland	Closed shrubland
Evergreen shrubland	Closed shrubland
Deciduous shrubland	Closed shrubland
Grassland	Grassland
Lichens and mosses	Grassland
Sparse vegetation (tree, shrub, herbaceous cover) (<15%)	Open shrubland
Sparse shrub (<15%)	Open shrubland
Sparse herbaceous cover (<15%)	Open shrubland
Tree cover, flooded, fresh or brakish water	Open shrubland
Tree cover, flooded, saline water	Open shrubland
Shrub or herbaceous cover, flooded, fresh/saline/brakish water	Open shrubland
Urban areas	Urban
Bare areas	Bare ground
Consolidated bare areas	Bare ground
Unconsolidated bare areas	Bare ground
Water bodies	Water